The Relative Stress-Corrosion-Cracking
Susceptibility of Candidate Aluminum-Lithium
Alloys for Aerospace Structural Applications

Patrick P. Pizzo

Advanced Research and Applications
Corporation

NASA

The Relative Stress-Corrosion-Cracking
Susceptibility of Candidate Aluminum-Lithium
Alloys for Aerospace Structural Applications

Patrick P. Pizzo

Advanced Research and Applications
Corporation
1223 E. Arques Avenue
Sunnyvale, California 94086

NASA

National Aeronautics and
Space Administration

Ames Research Center
Moffett Field. California 94035

TABLE OF CONTENTS

LIST OF ILLUSTRATIONS

2

LIST OF TABLES

ABSTRACT

The aging response of two powder metallurgy (P/M) pro-
cessed aluminum-lithium alloys has been determined. Alloy I
has the composition of Al-2.6% Li-1.4% Cu. Alloy II is the
same as Alloy I but also contains 1.6% Mg. Yield and ultimate
tensile strengths of 480 MPa and 550 MPa were obtained for Al-
loy I after a peak age of 26 hours at 443K. Higher yield and
ultimate strength of 525 MPa and 580 MPa were obtained for Al-
loy II after a peak age of 26 hours at 453K. Strain-to-fracture
was comparable for both alloys at about 3%. Some improvement
in tensile ductility was achieved at the sacrifice of tensile
strength by varying the solution heat treatment temperature
or by under-aging or over-aging. In general, fracture character-
istics were brittle, and limited reduction-in-area was observed
in both alloys. The fracture mode and morphology of the two
alloys differed. Alloy I fractured by transgranular separation
(slip-plane decohesion) along a plane of maximum shear stress.
Alloy II fractured by intergranular separation along a plane of
maximum tensile stress. A fixed orientational relationship was
found to exist between the shear fracture plane of Alloy I speci-
mens and the rolling direction, thus suggesting that this P/M
alloy may be strongly textured. Alloy II exhibited recrystalliza-
tion and grain growth, as well as coarse precipitation along grain
boundaries. The aging response of both alloys was found to be
sensitive to hot working operations performed prior to solution
heat treatment.

5

INTRODUCTION

Over the next decade, emphasis will be placed on the development of advanced aluminum alloys for aerospace structural applications.[1,2] Advanced alloys will be utilized in the design or major redesign of space, missile and aircraft systems. Alloys will be tailored in terms of: 1) density, 2) elastic modulus, and 3) strength to achieve major savings in weight and, thus, reduce operational expense. To fully assess the strength-to-weight or stiffness-to-weight advantage of the candidate alloys, durability criteria, such as fatigue endurance and/or environmental degradation, must be assessed. Stress corrosion cracking (SCC) of high-strength aluminum alloys has been a prevalent service problem in the aircraft industry. Thus, the strength-to-weight advantage for an alternative alloy needs to be normalized in terms of susceptibility to SCC. The purpose of the current research program is to: 1) identify a practical SCC screening technique, and 2) evaluate the relative SCC resistance of Al-Li candidate advanced aluminum alloys. This work is essential for successful near-term use of improved alloys for commercial systems and for the eventual development of optimum structural alloys.

The objective of this first report is to characterize the microstructure and tensile properties of the two aluminum-lithium alloys selected for study. The alloys were produced using the powder metallurgy technique. Due to the unique chemistry and fabrication history of the alloys, the decision was made to 1) investigate the aging response and 2) establish baseline tensile properties. The aging response was studied to determine the heat treatment sequence which will yield optimum mechanical properties. Particular attention was focused on achieving sufficient tensile elongation at high tensile strength so that degradation under SCC conditions could be properly assessed. The fracture morphology under ambient conditions was also characterized for later comparison to SCC features.

6

BACKGROUND

The two most widely used structural aluminum alloys in
the aerospace industry are the Al-Cu base alloy 2024 (Aluminum
Association designation) and the Al-Zn-Mg-Cu base alloy 7075.
In the aged condition (-T3 and -T4 for 2024 aluminum and -T6
for 7075 aluminum), the alloys are characterized by low smooth
specimen SCC threshold stress values (< 55 MN/m^2) in the short-
transverse direction.[3] This low resistance to SCC has resulted
in a high frequency of service problems. Through manipulation
of minor element chemistry and through alternate temper treat-
ments (overaging treatments), the SCC resistance of these alloys
has been improved, but usually at the expense of reduced tensile
properties. Additional progress has been made to introduce im-
proved alloys through adjustment of alloy chemistry and through
thermomechanical treatment (TMT). However, conventionally-pro-
cessed (cast ingot metallurgy) alloys fall short of demonstrating
sufficient improvement in properties to displace the two mainstay
alloys of the aerospace industry; the 2XXX and 7XXX series alloys.

Better combinations of strength, resistance to stress corro-
sion cracking and resistance to exfoliation corrosion can be
obtained in wrought products made from pre-alloyed atomized pow-
der than in corresponding products made from cast ingot. [2,4,5]
Improvements are attributable to the unique microstructure of the
rapidly solidified powders. Microstructural advantages include
1) decreased grain size (grain sizes less than 1 μm are attain-
able), 2) increased solid solubility (often by orders of magnitude
when compared to equilibrium conditions), and 3) elimination of
segregated phases. In the United States, microstructural char-
acterization of several base systems is proceeding. Aluminum
alloys that have been investigated include: Al-Cr, Al-Cu, Al-Fe,
Al-Co, Al-Ni, Al-Mn, Al-Zr, Al-Hf, Al-Fe-Mn, and Al-Mg-Mn. [2]
Microstructure and mechanical properties measurements on con-
solidated material are also being conducted. The following
alloys have been studied: Al-Cu-Mg (2024), Al-Zn-Mg (7075),
Al-Fe, Al-Mn-Cu, Al-Mn, Al-Cu-Mg-Li (2024 + lithium), Al-Li,
Al-Cu-Li and Al-Mg-Li. [1,2,5,6,7]

7

Alloy MA87, similar in composition to 7075 aluminum, is an
example of the potential alloy advancement available through P/M
techniques. In comparison with the ingot metallurgy (IM) 7075
aged to similar longitudinal yield strength, P/M alloy MA87 exhi-
bits an approximate 15% improvement in tensile strength, a 20%
improvement in the fatigue endurance limit, a reduced fatigue
crack growth rate, and a 100% increase in the resistance to
stress corrosion.[5] Powder metallurgy technology offers a broad
range of compositional variation, unattainable through conven-
tional cast ingot processing. Thus, the greatest potential for
significant advancement in aluminum aerospace alloys may be
provided by P/M processing technology.

Of the many candidate aluminum structural alloys being de-
veloped using P/M technology, aluminum-lithium alloys offer the
best potential for successful near-term use in the aerospace
industry. Al-Li alloys are prime candidates because they offer
significant increases in specific modulus (i.e., elastic modulus
to density ratio), while providing strength similar to the 7XXX
series and 2XXX series I/M alloys.[1,7] Because difficulties have
been experienced in conventional casting, alloy X-2020 (Al-4.5
Cu-1.5 Li)* was withdrawn as a commercial product in the late
1950's. Recent attention has focused on producing Al-Li alloys
from rapidly solidified powders.[2,6]

Two powder metallurgy processed Al-Li alloys have been pro-
cured for the SCC study. The alloys are Al-2.6% Li-1.4% Cu and
Al-2.6% Li-1.4%Cu-1.6% Mg. Both compositions are of potential
commercial interest because of the high specific strength values
attainable. In addition, the presence of magnesium in the latter
alloy alters the precipitation kinetics and influences the size
and distribution of the grain boundary precipitates. Since grain
boundary precipitates and/or the accompanying precipitate free
zones (PFZ's) are thought to play an important role in the stress
corrosion cracking process, the influence of the Mg addition will
be closely monitored.

*All compositions in weight percent

8

EXPERIMENTAL TECHNIQUE

Two aluminum-lithium alloys were purchased from Kawecki Berylco Industries, Inc., Reading, Pennsylvania. The alloys were processed using powder metallurgy (P/M) techniques. Powders were produced by rapid cooling an atomized molten stream of the target composition in an inert gas (Ar) atmosphere. High-purity (0.9999 weight percent) aluminum and a 20 wt. pct. lithium master alloy were combined so as to yield an approximate 2.6 wt. pct. aluminum-lithium melt. High purity element additions were made to adjust the melt to the desired alloy composition. The cooling rate of the atomization process was estimated to be approximately 10^3 °K/sec. The resulting powders were spherical, about 150 m in diameter (sized to 100 mesh).

Powders were packed in 6061 aluminum cans (13.7 cm O.D. with a 0.32 cm wall) and cold isostatic pressed to 415 MPa. The compacted powders were then hot upset at 755°K against a blind die and extruded at 672°K through a 55.9 mm by 1<.7 mm (2.2 inch by 0.58 inch) die. This yields an approximate 10:1 extrusion ratio.

The chemical compositions of the resulting alloys are presented in Table I. The lithium content was determined using the wet chemical technique. The zirconium is added to refine grain size and to retard grain growth. The Al- Li- Cu alloy is hereafter designated Alloy I. The Al- Li- Cu- Mg alloy is hereafter designated Alloy II.

Microstructures representative of the as-received alloys are presented in Figure 1. Coarse precipitation is observed in both alloy systems and this results from the somewhat high processing temperatures used in the consolidation of the powders. The precipitation in Alloy II is particularly coarse. Precipitation is found to be preferentially in lines parallel to the extrusion direction (ED) in both alloys, although the effect is most notable in Alloy I.

9

To scope the aging response of the alloys, hardness testing was conducted on coupon specimens 12 mm by 8 mm by 1.5 mm, cut from hot rolled strip. The strip was hot rolled at about 700°K with rolls maintained at 450°K. The section thickness was reduced about 5% per pass, and the material was reheated to 700°K after every four passes. In this manner, a 1.5-mm-thick strip was prepared from the 14.7 mm thick original extrusion and was also used to make tensile specimens for characterization of the mechanical properties. The Rockwell 15-T superficial hardness scale was used to measure hardness.

Tensile tests were performed using the three specimen types depicted in Figure 2. The tensile coupons, Figure 2a, were also fabricated from the hot rolled strip. The straining electrode specimens (for the subsequent stress corrosion study), Figure 2b, and the tensile rounds, Figure 2c, were fabricated from the extruded plate. All heat treating was performed in air after specimen fabrication. Specimens were rough-polished to 600 grit abrasive paper prior to testing. Tensile tests were performed using a closed loop electrohydraulic test system under stroke control. Tensile tests were conducted under ambient conditions at a measured plastic strain rate of $1.4 \times 10^{-4}s^{-1}$. Modulus determinations were made from the output of two strain gauges attached to opposite sides of tensile coupons, Figure 2a. An extensometer was used to determine engineering strain, e, to final fracture. The strain-to-fracture, ^{e}f, data reported herein are the values of the plastic engineering strain-to-fracture determined from the displacement versus load record.

RESULTS AND DISCUSSION

In this section, the microstructure, aging response, and
tensile properties of the two aluminum-lithium alloys are char-
acterized. First, attention is focused on microstructural
changes occurring as a result of heat treatment and hot rolling.
Solution heat treatment was necessary to dissolve the coarse
$\delta(Al_3Li)$ precipitates found in the as-received material and
condition the alloy for peak age-hardening. Second, the aging
data are presented. Time and temperature conditions for peak
strengthening are defined for each alloy. Next, the tensile
properties of Alloys I and II are presented as a function of
heat treatment. The purpose of these data is to establish
strength/ductility combinations which are most pertinent for
the subsequent investigation of stress corrosion cracking.
Finally, the morphology of room temperature fracture is also
characterized to assist interpretation of the tensile results
and for later comparison to fractures induced by stress cor-
rosion cracking.

Microstructure

Solution heat treatment was performed to dissolve the
coarse precipitates found in the P/M processed alloys. Pre-
liminary scoping tests indicated that the precipitates begin
to go into solution at temperatures somewhat greater than $670^{o}K$.
This is consistent with the solubility data for the binary Al-Li
alloy system reported by Costas and Marshall.[8] Thorough disso-
lution of precipitates within 0.5 hours occurred for tempera-
tures greater than $780^{o}K$. Solution heat treat conditions
ranging from 768° to $828^{o}K$ are investigated in this study.

Aging Response

Many aluminum alloys exhibit age hardening due to the growth of metastable phases that result from decomposition of the supersaturated solid solution. The metastable phase responsible for strengthening in Al-Li binary alloys is an ordered Al_3Li precipitate, termed δ'. [9,10] Under certain conditions of time and temperature, the precipitation of δ' is homogeneous, producing a high density of very small ($\sim$.010μm diameter) spherical precipitates. In Al-Li-Cu ternary alloys, the lithium precipitates independently of copper which follows the sequence that occurs in the Al-Cu binary system:

$$GPI \longrightarrow GPII \longrightarrow \theta'' \longrightarrow \theta' \ (Al_2 \ Cu)$$
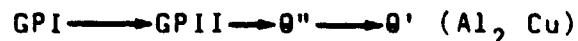
Both the δ' and the θ'' precipitates effectively impede dislocation motion, causing an increase in flow strength. However, continued aging results in progressive loss in coherency between the matrix and the precipitate as the metastable δ' transitions to δ phase and as the θ'' proceeds toward the equilibrium θ'. As a consequence, there is a reduction in yield and tensile strength, as predicted by mechanisms such as the one proposed by Orowan. [11] Maximum strengthening thus occurs at some intermediate aging time that is dependent, in part, on alloy chemistry. In this section, data which characterize the aging response of the two alloys are presented.

The microstructures of Alloy I and II, after solution
heat treatment at 828°K for 0.5 hours, are presented in
Figures 3 and 4. Linear indications present in the original
extrusion remain decorated with precipitates. Recrystalliza-
tion is observed in both alloys. The larger recrystallized
grains are about 30µm long in the extrusion direction, while
growth in the short transverse direction appears constrained
by the linear array of precipitates. The array of precipitates
is linear rather than planar. This is also evident in the trans-
verse section micrographs of Figure 4. A relatively uniform
array of precipitates is observed in the transverse field. The
recrystallized grains are rather equiaxed and of the approximate
dimension of the spacing of the linear indications in the longi-
tudinal section. The linearly-aligned precipitates of Figure 3
are thought to be zirconium. This will be investigated in later
work.

The microstructure of the hot rolled strip after 828°K/0.5-
hour solution heat treatment and subsequent aging is presented
in Figure 5 for Alloy I and in Figure 6 for Alloy II. Both
longitudinal and transverse sections are presented. Alloy I is
found to retain microstructural features refined by the hot
rolling process. Grains and/or sub-grains approximately 5µm in
size are observed in Figure 5b. On the other hand, extensive
recrystallization and grain growth is observed in the magnesium-
containing alloy, Alloy II. The structure of Alloy II consists
cf large grains (> 100µm diameter) amongst local clustering of
smaller, equiaxed grains. Coarse precipitates are observed
along grain boundaries. The possibility of heterogeneous pre-
cipitation of a grain boundary phase will be investigated in
a subsequent transmission electron microscopy study. Large
(60µm long) particles, such as that in Figure 5a, are present
in both aluminum-lithium alloys. Energy dispersive analysis
(KEVEX) indicates the particles contain Al and/or Li. The par-
ticles may relate to the master alloy addition and are probably

13

carryovers from the melt during the atomization process. The point of fracture initiation in approximately 10% of the tensile tests was associated with such particles.

The aging response of Alloys I and II is presented in Figures 7 through 9. Figure 7 is a plot of hardness as a function of aging temperature for a constant aging time of 16 hours. These data define the temperature regime where the δ'/θ'' precipitation is r?·id; they also provide a measure of the relative strength difference between Alloys I and II. Figures 8 and 9 show the variation in hardness with time for two aging temperatures; $443^{\circ}K$ and $463^{\circ}K$ respectively. Since hardness is a measure of the yield and flow strength of an alloy, the data indicate time/temperature conditions for maximum strengthening. The data of Figure 7 indicates that accelerated strengthening occurs at a higher temperature for the magnesium bearing alloy, Alloy II. For a fixed aging time, maximum hardening occurs at $450^{\circ}K$ for Alloy I and at $470^{\circ}K$ for Alloy II. The magnesium addition appears to alter the precipitation process and increase the strength of the base alloy. On the basis of the data of Figure 7, aging temperatures of $443^{\circ}K$ and $463^{\circ}K$ were selected for the time-at-temperature aging study. The time dependence of hardness for aging Alloys I and II at $443^{\circ}K$ and $463^{\circ}K$ are reported in Figures 8 and 9, respectively. Peak hardness for Alloy I occurs in about 30 hours at $443^{\circ}K$. Alloy II reaches full hardness in about 200 hours at this temperature. At $463^{\circ}K$, Alloy I is peak aged in about 5 hours while Alloy II requires 40 hours to attain maximum hardness. The addition of magnesium is again demonstrated to increase alloy strength and to alter precipitation kinetics.

Tensile Properties and Fracture Morphology
The goal of this study was to develop a heat treatment which will render the reference alloys high strength and yet maintain sufficient and reproducible ductility, about 6%, to perform the SCC investigation. In this section, the baseline tensile properties of Alloys I and II are presented as a function of aging condition. The tensile properties are characterized in Figures 10 thru 14 and in Table 2.

14

In Figures 10 and 11, the yield strength (0.2% offset), ultimate tensile strength and plastic strain-to-fracture versus aging time curves for Alloys I and II, respectively, are presented. Tensile coupons, Figure 2a, were used. Curves for $443^{o}K$ and $463^{o}K$ aging are presented in each figure. The following trends are observed:

1) The largest value of strain-to-fracture at relatively high strength is 5% for Alloy I and 6% for Alloy II.

2) While the strain-to-fracture, e_f versus $443^{o}K$ aging curve for Alloy I (Figure 10) goes through a minimum as peak aging is approached, the $463^{o}K$ aging curve for e_f exhibits an unexpected maxima.

3) The e_f versus $463^{o}K$ aging curve for Alloy II exhibits a local maxima at about 14 hours. As the peak strength is more closely approached, the strain-to-fracture rapidly decreases.

4) The yield strength and ultimate tensile strength versus aging time curves of Figures 10 and 11 correlate well with the hardness versus aging curves of Figures 8 and 9. Aging peaks occur at similar aging times.

The data of Figures 10 and 11 point out the necessity for close control of aging conditions because of the anamolous behavior of the ductility parameter, e_f. The optimum e_f value of 5% for Alloy I can be attained either by peak aging at $463^{o}K$ or by overaging at $443^{o}K$. A strain-to-fracture value of 6% results when Alloy II is underaged, but if aging proceeds too far, the strain-to-fracture rapidly declines to about 3%. Aging temperatures somewhat greater than $463^{o}K$ are expected to shift the aging response curve to the left such that the decline in e_f with time may occur for significantly shorter times. The reproducibility of ductility parameters is a major concern in the SCC study. Therefore, the e_f for selected heat treatments will require a statistical base to define reproducible control conditions.

To determine Young's modulus, E, strain gauges were mounted on two sides of the flat tensile coupons. Moduli are reported in Table 2. A value of 80 GPa is consistent with the data of Webster on alloys of similar composition.[12] The modulus for 7075-T6 aluminum is included for comparison. The reference aluminum-lithium alloys are 12% stiffer than 7075-T6 aluminum.

The morphology of the fractured tensile test specimens was studied for later comparison to stress corrosion fracture surfaces. Photographs of the tensile coupon fractures are presented in Figures 12 thru 16.

Alloys I and II were observed to fail in distinctly different manners as illustrated in Figure 12 where typical fracture surfaces are shown. Figure 12a is a comparison of the fracture profile of Alloy I (top) and Alloy II fractures. Alloy I fails by shear (47.5° measured with respect to the load axis) while Alloy II fractures on a plane perpendicular to direction of maximum load. Shear fractures for Alloy I and tensile fractures for Alloy II were observed for the specimens used to generate the data of Figures 10 and 11. Comparison of the fracture surfaces of Alloys I and II is presented in Figure 12b. The variation in fracture topography is clearly observable.

In Figures 13 and 14, scanning electron micrographs (SEM) showing the fracture topography of Alloy I specimens are presented. A stepped, brittle fracture appearance is observed. Elongated dimples, characteristic of ductile metals failed by shearing, are not observed.

SEM micrographs of the fracture surface of Alloy II spec-
imens are presented in Figures 15 and 16. The fracture of the
magnesium-bearing alloy contains laminar tears oriented paral-
lel to the rolling plane. The tears are thought to occur along
interfaces weakened during processing of the hot rolled strip.
In substantiation, fracture surfaces of Alloy II specimens fab-
ricated from the as-received extrusion do not exhibit laminar
tears. Intergranular facets approximately $5\mu m$ in size are the
predominant fractographic feature.

Both Alloy I and Alloy II fractures exhibit less than 3%
reduction in area . In addition, final fracture of the tensile
specimens occurs at the point of plastic instability (maximum
load). These data combined with the SEM fractographic results
demonstrate the brittle nature of fracture in both alloys.

The tensile data of Figures 10 and 11 represent Al-Li al-
loy solution heat treated at $828^{\circ}K$. In Figures 17 and 18,
tensile properties are presented as a function of solution heat
treatment temperature for a constant aging condition. These
data were obtained using tensile round specimens,· Fig. 2(c),
which were fabricated directly from the extruded plate. The
objective of these tests was to determine the solution heat
treatment (SHT) which provides optimum ductility for each of
the alloys. The following results are found:

(1) The ductility of Alloy I is somewhat greater than 3%
    and unaffected by SHT temperature. However, the yield
    strength (YS) and ultimate tensile strength (UTS) are
    maximum at $788^{\circ}K$. These data suggest that the aging
    response of Alloy I solution heat treated at $788^{\circ}K$ be
    investigated for optimum properties.

(2) The ductility of Alloy II decreases and the
    strength values, YS and UTS, increase as the SHT
    temperature is increased. Thus, the optimum SHT
    is a compromise between strength and ductility
    requirements. SHT at 788°K produces material
    with 469 MPa yield strength, 550 MPa ultimate
    tensile strength, and an elongation-to-fracture
    value of 5%; excellent tensile properties.

(3) Values of strength for the 828°K SHT condition
    for both alloys are higher than corresponding data
    reported for the tensile coupons. The yield
    strength and UTS values of Alloy I are 9% greater.
    For Alloy II, there is a more pronounced affect;
    tensile round YS and UTS data are greater by 42%
    and 30%, respectively. This anomaly will be dis-
    cussed later in this report.

Fracture characteristics for the tensile rounds are
analogous to those of the flat tensile coupons, and this is
illustrated in Figure 19. Alloy 1 fracture occurs along the
plane of maximum shear stress and Alloy II fracture occurs
along the plane of maximum tensile stress. For Alloy II ten-
sile rounds, there were two exceptions; both the specimen solu-
tion heat treated at 768°K and a specimen in the as-extruded
condition fractured along the plane of maximum sheur stress.
This translation in fracture behavior in Alloy II is attributed
to two reasons:

(1) For SHT temperatures less than 783°K, dissolu-
    tion of coarse preciptates is incomplete, and
    recrystallization and grain growth do not occur.
    Thus, the as-extruded and 768°K SHT specimens

18

differ from the remaining Alloy II specimens in that relatively large, equiaxed grains are not present (compare Figure 1 to Figure 3).

(2) For SHT temperatures in excess of $783^{\circ}K$, coarse grain boundary precipitation accompanies recrystallization and grain growth in the magnesium-bearing alloy. The grain boundary precipitation significantly reduces the cohesive strength of the grain boundary regions.

To demonstrate that precipitation events are preponderantly responsible for the fracture transition observed for Alloy II, and for the more basic difference in fracture behavior between Alloys I and II, consider the SEM fractographs of Figures 20 and 21. The fracture topography of Alloys I and II are compared in Figure 20. Alloy I exhibits a relatively flat, featureless topography while Alloy II fractures intergranularly. The flat featureless regions, Figure 20(a), are thought to correspond to crystallographic slip planes along which deformation is localized in the Al-Li-Cu and Al-L-Cu-Mg alloy systems. Slip is constrained to slip bands due to the ordered nature of the δ' precipitates. Slip continues until pile-up stresses are sufficient to cause slip-plane decohesion. Both alloys are thought to have a strong preferred orientation and, thus, a relatively flat fracture topography is expected.

Alloy II also deforms by localized slip. However, large, closely-spaced grain boundary precipitates are present in the microstructure due to the magnesium addition (reference the optical micrographs of Figures 4 and 6). The coarse grain boundary precipitates reduce the cohesive strength of grain boundaries. A condition is reached where stresses generated at the tip of the slip bands during deformation are sufficient

19

to cause grain boundary decohesion in preference to slip plane decohesion and intergranular fracture results. The coarse nature of the grain boundary precipitates and their influence on final fracture are evident in the fractographs of Figure 21.

It has been shown that the tensile properties for round specimens, Figures 17 and 18, are considerably greater than corresponding properties for the flat tensile coupons, Figures 10 and 11, for an equivalent heat treatment. Indeed, the YS and UTS values for Alloy II are respectively 42% and 30% greater in comparing tensile round and coupon data. Since there is a processing difference as well as specimen size difference, further testing was performed to investigate this anomaly.

Tensile tests were performed on straining electrode specimens, Figure 2(b), which were fabricated directly from the as-extruded alloy, providing isolation of the processing variable. The resulting data are plotted in Figures 22 and 23. Interpretation of the data for Alloy II is complicated because the specimens were inadvertently duplex aged. The specimens were aged at $443^{\circ}K$ for the respective times indicated in Figure 23, prior to $463^{\circ}K$ aging. The data are nonetheless presented, for some useful information is obtainable. The data of Figures 21 and 23 indicate the following:

1. With the exception of the high-yield strength of the specimen aged for 3 hours at $463^{\circ}K$, the tensile strength for the Alloy I straining electrode and coupon-type specimens is comparable. However, the strain-to-fracture data are not consistent with the trend curve representing coupon type specimens. A trend of increasing ductility with decreasing tensile strength is indicated.

2. The strength parameters for the Alloy II straining electrode specimens, Figure 23, are directly comparable to values determined for tensile rounds, Figure 18; that is, YS and UTS values are substantially greater than values obtained from the hot rolled tensile coupons. Processira strongly influences Alloy II properties.

3. The duplex aging greatly accelerates δ ' precipitation in Alloy II. This is evident in that initial aging for short times at $445^{\circ}K$ (3 and 26 hours respectively), shifts the subsequent $463^{\circ}K$ aging response curve to shorter times. The aging peak is shifted from about 50 hours to less than three hours by duplex aging. The straining electrode spec- imen data in Figure 23 are consistent with an overaged con- dition for Alloy II.

The data of Figures 22 and 23 demonstrate the importance of processing as a control variable for the reference aluminium- lithium alloys. Variations in grain shape and size and the size and distribution of grain boundary precipitates strongly effect the mechanical behavior. Alloy II is more strongly affected because recrystallization and grain growth occur readily in this alloy, and grain boundary precipitation is apparently more extensive. Even in the case of Alloy I, where shear frac- ture mechanisms dominate, the data indicate the importance of the control of process history to yield reproductible ductility.

The fracture morphology of the straining electrode speci- mens was consistent with results obtained for coupon and tensile round specimens. Alloy I fractures were shear dominated, while Alloy II fractures occurred on a plane of maximum tensile stress. The fracture profile of an Alloy I straining electrode specimen is compared to tensile coupon fracture profile in Figure 24.

SEM fractographs representative of Alloy I and II are presented
in Figure 25. The brittle shear characteristics previously re-
ported for Alloy I were again observed. Alloy II fractures in-
tergranularly, and again grain facets are typically 5μm in size.
Secondary intergranular cracking is also observed.

Examination of the various shear fractures of the ten-
sile characterization program suggests that there is a strong
preferred orientation in the reference Al-Li alloys. This is
demonstrated in the facture comparison of Figure 24 and the
schematic of Figure 26. When orientations of the various ten-
sile specimens are compared, final fracture occurs on planes
preferentially oriented with respect to the rolling direction.
.X-ray diffraction will be used to determine the degree of tex-
ture and the preferred orientation.

SUMMARY

The reference aluminum-lithium P/M alloys do offer the
potential of high strength, high modulus and low density.
Strength properties of 480 MPa yield and 550 MPa ultimate
tensile strength with strain-to-fracture approaching 5% can be
achieved through proper thermo-mechanical treatment. However,
the P/M alloys investigated are characterized by limited
deformation beyond plastic instability. Very little reduction
in area is observed and fracture chacteristics are brittle.

Because intergranular fracture occurs in Alloy II during
tensile testing under ambient conditions, it is possible that
the tensile properties of this alloy are environmentally
sensitive. Thus, as a result of the tensile characterization-
program, the scope of the stress corrosion study has been
expanded to include slow-strain rate tests of Alloy II after
pre-exposure to a high humidity environment. Also, because of
the extent to which grain boundary precipitation occurs, Alloy
II is anticipated to be the more stress corrosion susceptible
of the two alloys.

Sufficient mechanical properties data have been generated
to characterize the tensile properties of the two reference
alloys. However, further tests are required to demonstrate
satisfactory reproducibility of properties for specimens to be
used in the stress corrosion program. The alloy processing
steps and heat treatment must be somewhat refined to assure
reproducible properties; in particular, strain-to-fracture
characterization tests are in progress.

23

CONCLUSIONS

1) Strength properties of 430 MPa yield and 550 MPa ulti-
mate tensile strength with strain-to-fracture approaching 5%
can be achieved in both reference aluminum-lithium alloys selected
for the stress corrosion study. These properties, combined with
the high elastic modulus (80 GPa), make both compositions viable
commercial candidates.

2) Reproducibility of properties requires close control of
both alloy processing and heat treatment parameters. Further tests
are required to demonstrate satisfactory reproducibility of proper-
ties for specimens to be used in the stress corrosion program.

3) Precipitation is more sluggish in Alloy II (Al-Li-Cu-Mg)
than in the Al-Li-Cu ternary alloy, Alloy I. However, greater peak
strength occurs in the magnesium-bearing alloy. A yield strength
of 525 MPa and ultimate tensile strength of 590 MPa with a 3% strain-
to-fracture value was attained for Alloy II. The maximum yield and
ultimate tensile strength attained in Alloy I are 480 MPa and 550
MPa respectively.

4) Alloy I fractures along a plane of maximum shear stress,
while Alloy II, in general, fractures on a plane of maximum tensile
stress. Alloy II fractures intergranularly, while Alloy I fractures
via slip-plane decohesion.

5) For equivalent thermomechanical processing, recrystalli-
zation and grain growth is more extensive in the magnesium-bearing
alloy, Alloy II.

6) It appears that .09 wt. pct. Zr is insufficient to
retard grain growth, particularly in the magnesium-bearing alloy.

7) The P/M aluminum-lithium alloys are characterized by limited deformation beyond plastic instability. Very little reduction in area is observed and fracture characteristics are brittle.

8) A fixed orientational relationship between tensile fracture surfaces and the rolling direction suggest that the P/M processed alloys are stongly textured. This is being investigated in ongoing study.

9) Because of the intergranular nature of fracture in tensile tests in Alloy I under ambient conditions, tensile properties may be environmentally sensitive. Slow strain rate tests will thus be performed for Alloy I specimens prexposed to a high humidity environment.

REFERENCES

1) Sanders, T. H. and Balmuth, E. S., "Aluminum-Lithium Alloys: Low Density and High Stiffness," *Metal Progress*, *113*, Nr. 3 (1978).

2) Lewis, R. E., et. al., "A Feasibility Study for Development of Structural Aluminum Alloys from Rapidly Solidified Powders for Aerospace Structural Applications," Final Report AFML-TR-78-102, Lockheed Research Laboratory, Palo Alto, California, Contract F33615-77-C-5186 (May 1978).

3) Speidel, Markus O., "Stress Corrosion Cracking of Aluminum Alloys," *Met. Trans.*, *6A* (April 1975) p. 631.

4) Lyle, J. P., Cebulak, W. S. and Buchovecky, K. E., "Progress in Powder Metallurgy," *28*, Metal Powder Industries Federation, N.Y., 1972, p. 93

5) Lyle, J. P. and Cebulak, W. S., "Program Metallurgy Approach for Control of Microstructure and Properties in High Strength Aluminum Alloys," *Met. Trans.*, *6A* (April 1975), p. 685.

6) Sankaran, K. K., "Structure and Properties of Splat-Quenched 2024-Type Al Alloys Containing Li," Ph.D. Thesis, MIT, Cambridge, Mass., 1978.

7) *Proceedings of The First International Conference on Aluminum-Lithium Alloys*, Stone Mountain, Georgia, May 19-21, 1980, to be published.

8) Costas, L. P. and Marshall, R. P., Trans. AIME, *224* (1962), p. 970-974.

9) Noble, B. and Thompson, G. E., *Metal Science Journal*, *4*, No. 12, (Dec. 1968), P. 35-43.

10) Tamura, M., Mori, T. and Nakamura, T., <u>J. of Jap. Inst. of Met.,</u>
    <u>31</u> (.970), p. 919.

11) Orowan, E., Nye, J. F. and Cairns, W. J., M.O.S. Armament Research
    Dept. Rep. (16/45), (1945), p. 35.

12) Webster, D., <u>Met. Trans.,</u> <u>10A</u> (Dec. 1979), p. 1913.

(a)

30μm

E.D.

(b)

30μm

E.D.
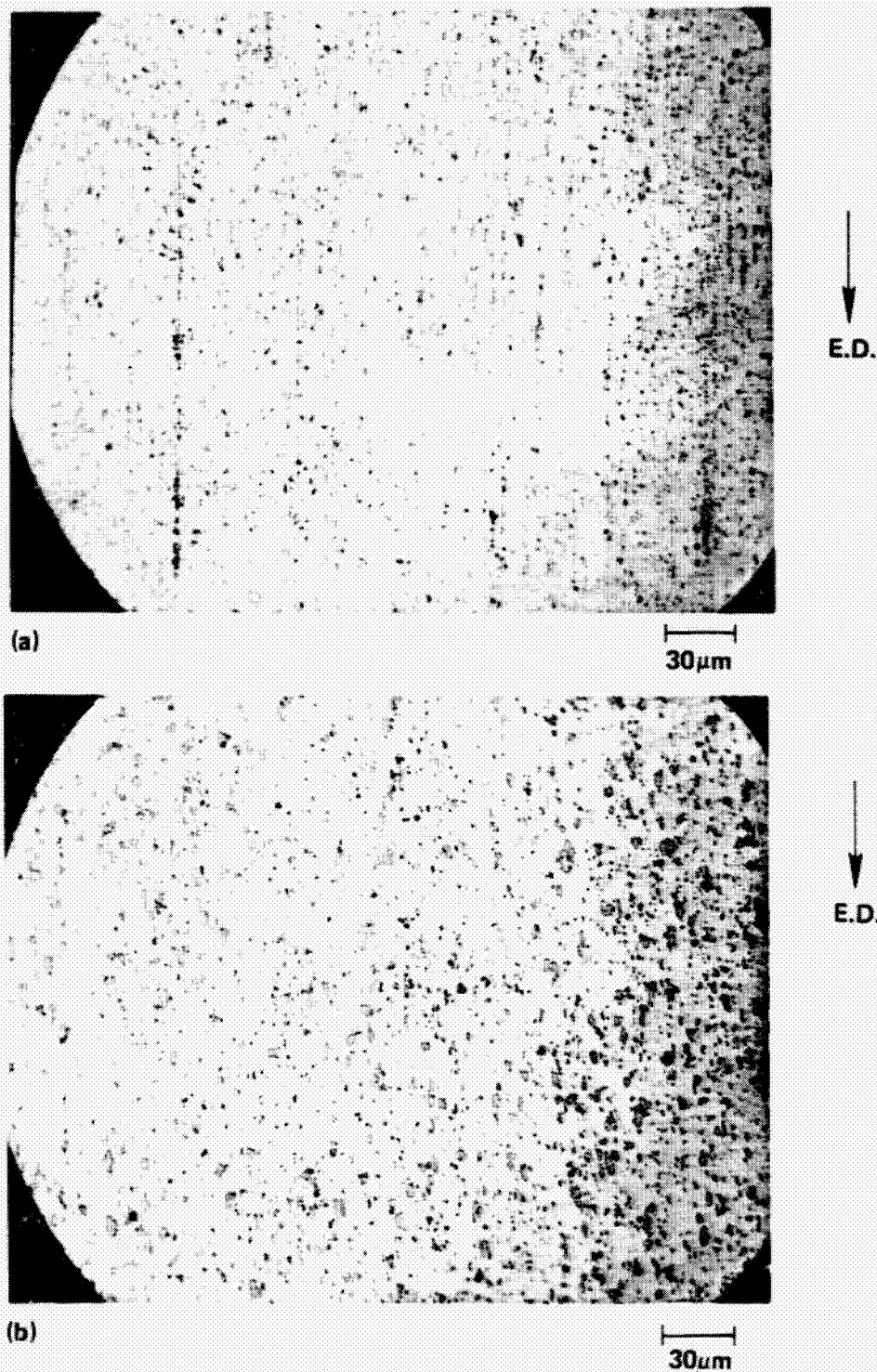
Fig. 1: Representative microstructure of the extruded plate
(extrusion direction, E.D., indicated) (a) Alloy I
(Al-2.6 Li-1.4 Cu) (b) Alloy II (Al-2.6 Li-1.4 Cu-1.6 Mg).
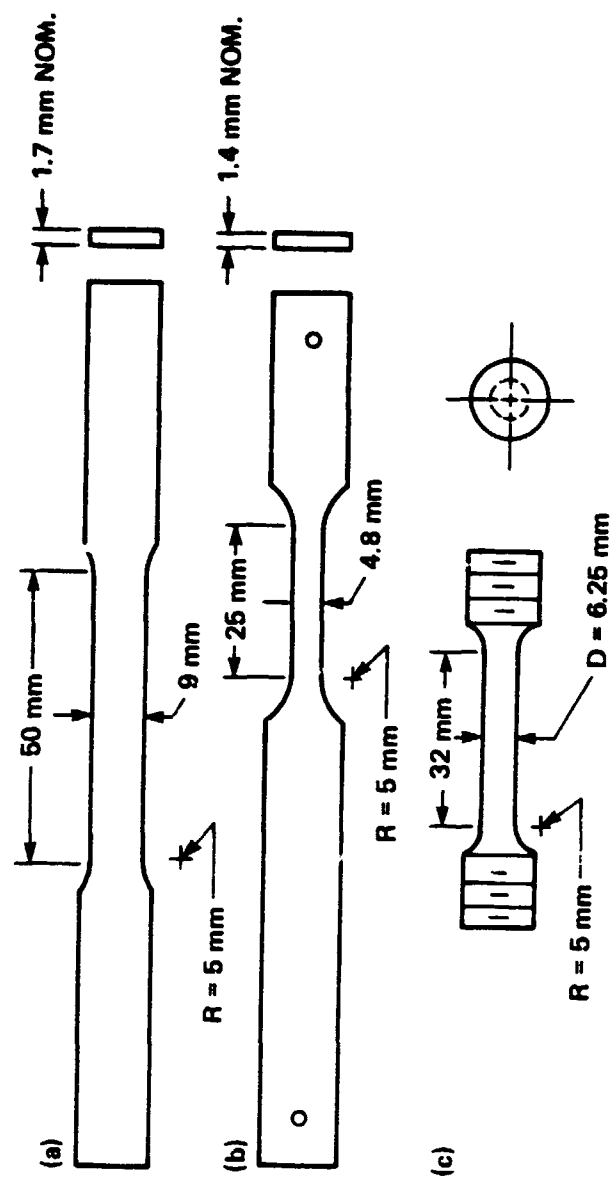
Fig. 2: Specimen types used to characterize the tensile properties of the Al-Li alloys (a) tensile coupon (b) straining electrode specimen (c) tensile round.

29

(a)

20μm

(b)
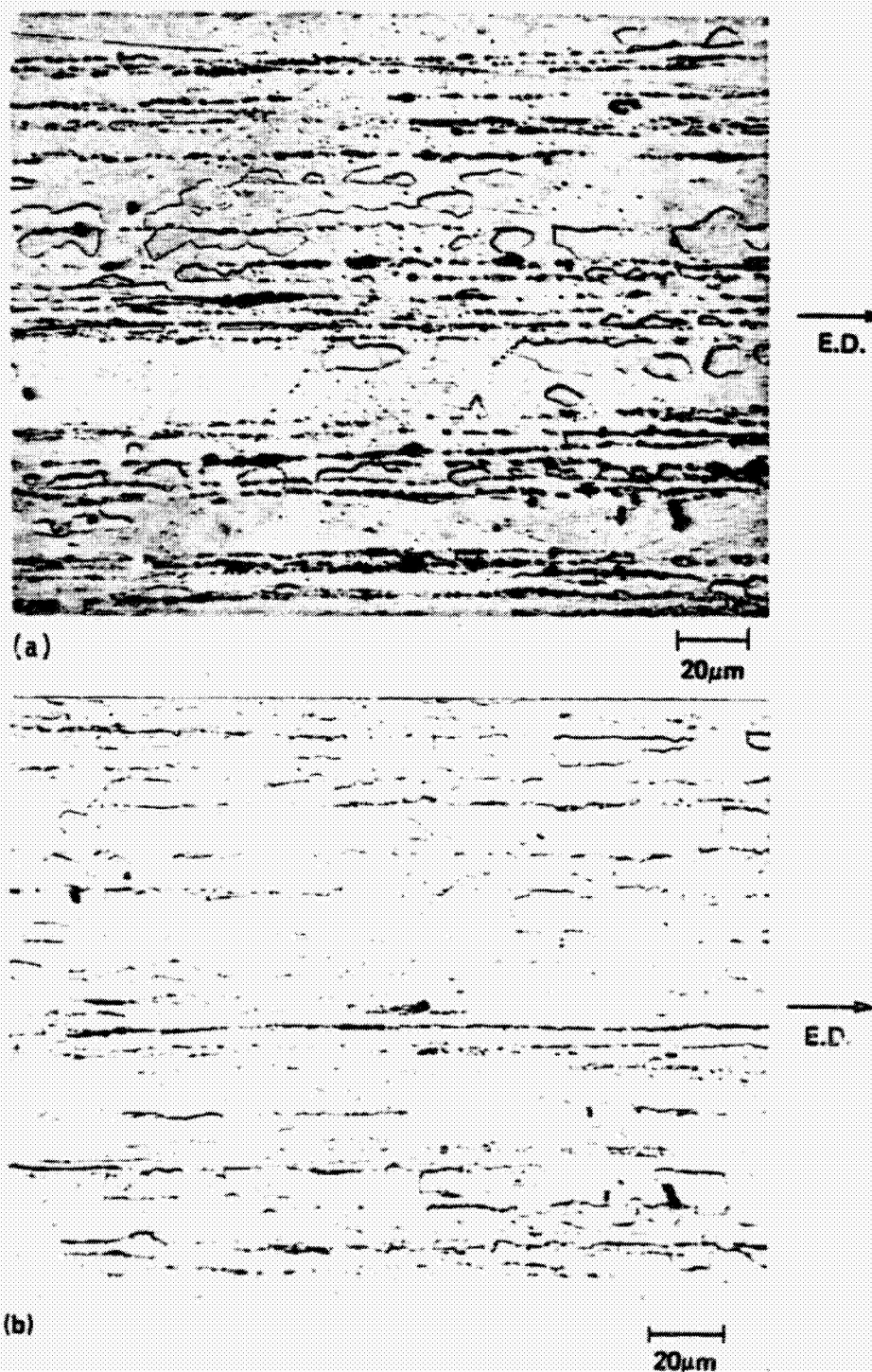
20μm

Fig. 3: Representative microstructure of the extruded Al-Li alloy plate after solution heat treatment (828K for 0.5 hours) - longitudinal sections (a) Alloy I (b) Alloy II.

(a)

⊗ E.D.

├──┤ 20μm

(b)

⊗ E.D.
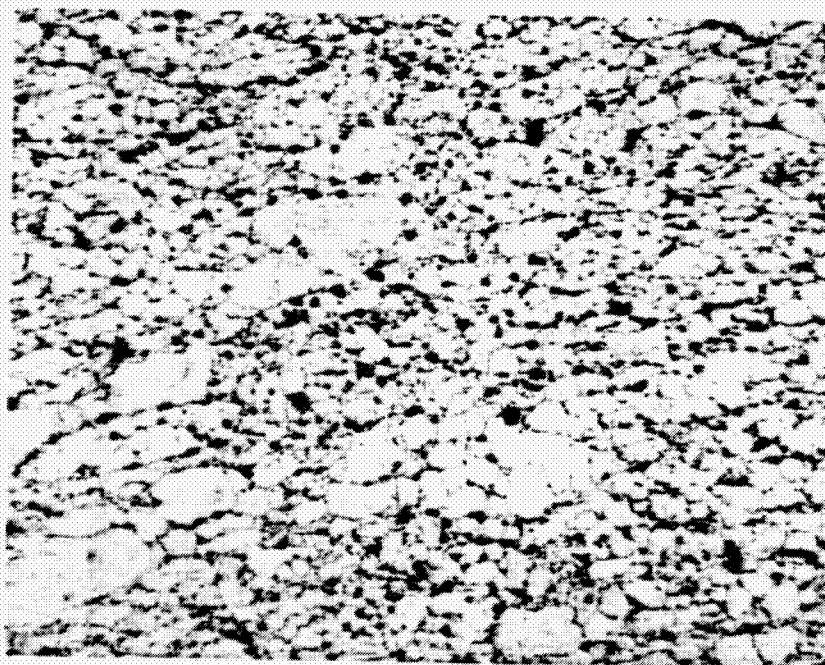
├──┤ 20μm

Fig. 4: Representative microstructure of the extruded Al-Li alloy plate after solution heat treatment (828K for 0.5 hours) - transverse sections (a) Alloy I (b) Alloy II.

R.D.

(a)

30μm

(b)
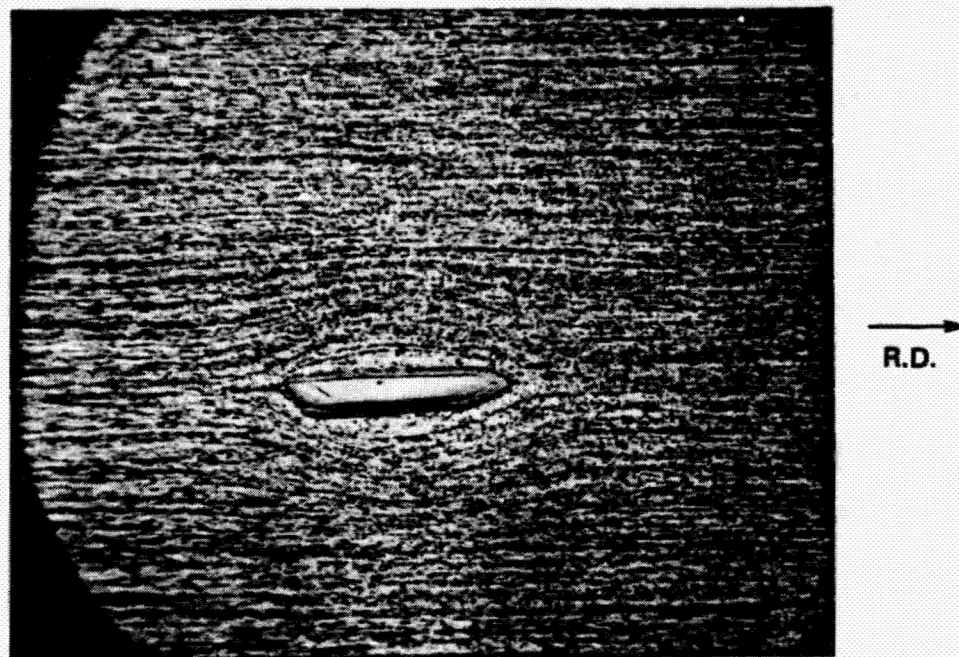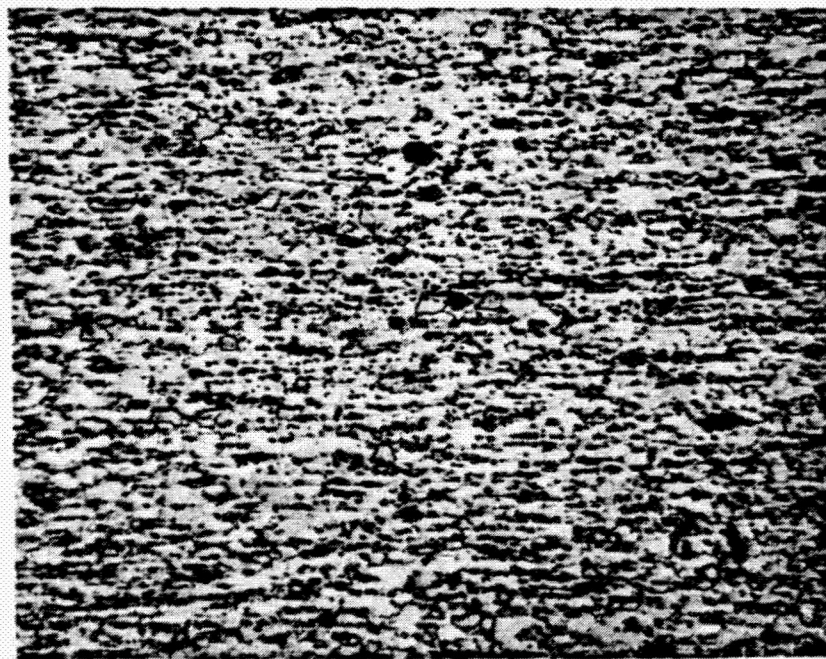
20μm

Fig. 5: Representative microstructure of the hot-rolled
Alloy I sheet, solution heat treated at 828K for 0.5
hours and aged 5 hours at 463K (rolling direction,
R.D., indicated) (a) longitudinal section and (b)
short-transverse section.

R.D.

(a)

40μm

(b)

20μm
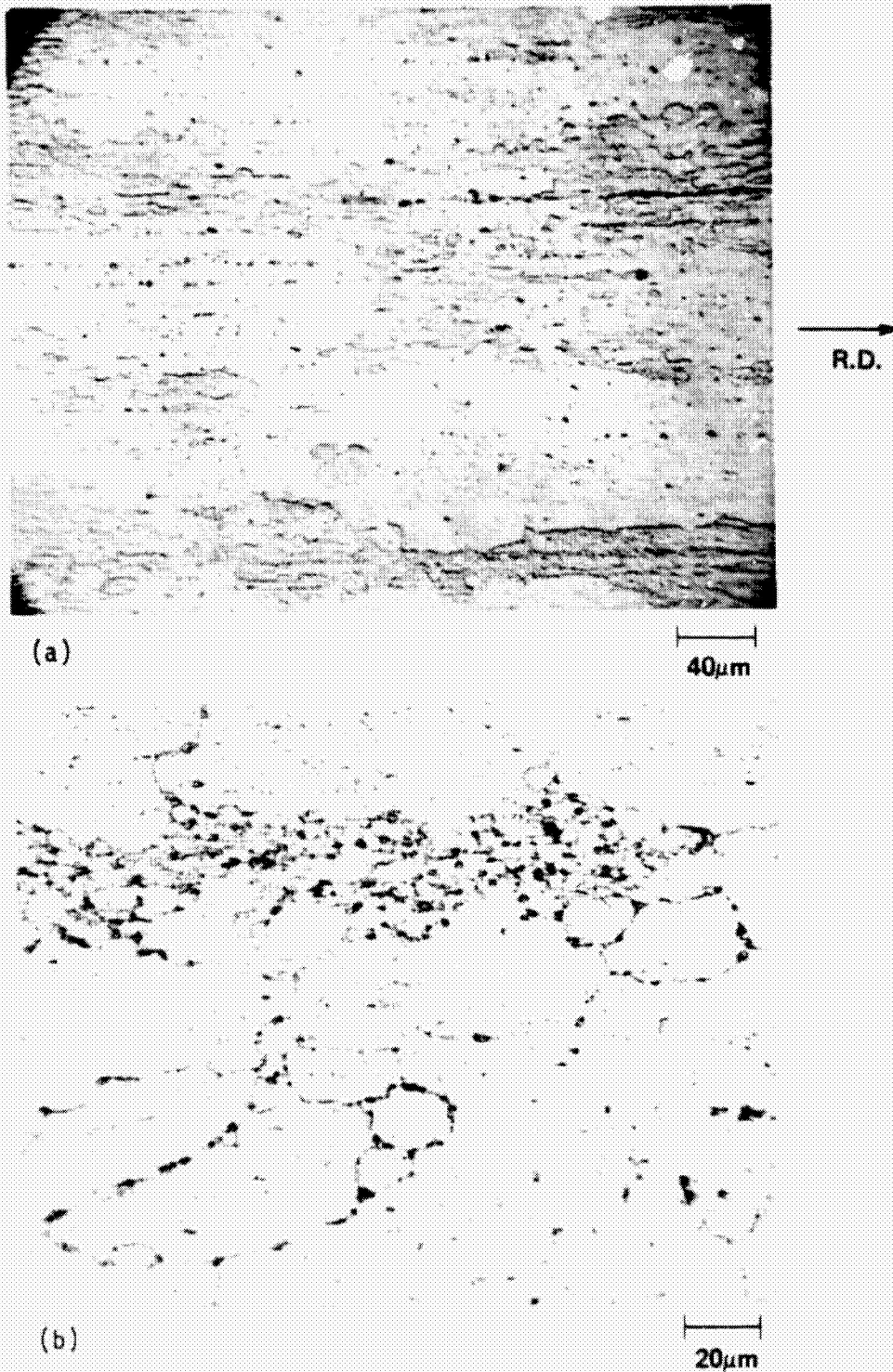
Fig. 6:   Representative microstructure of the hot-rolled
          Alloy II (magnesium bearing alloy) sheet; solution
          heat treated at 828K for 0.5 hours and aged 20 hours
          at 463K (a) longitudinal section and (b) short-
          transverse section.
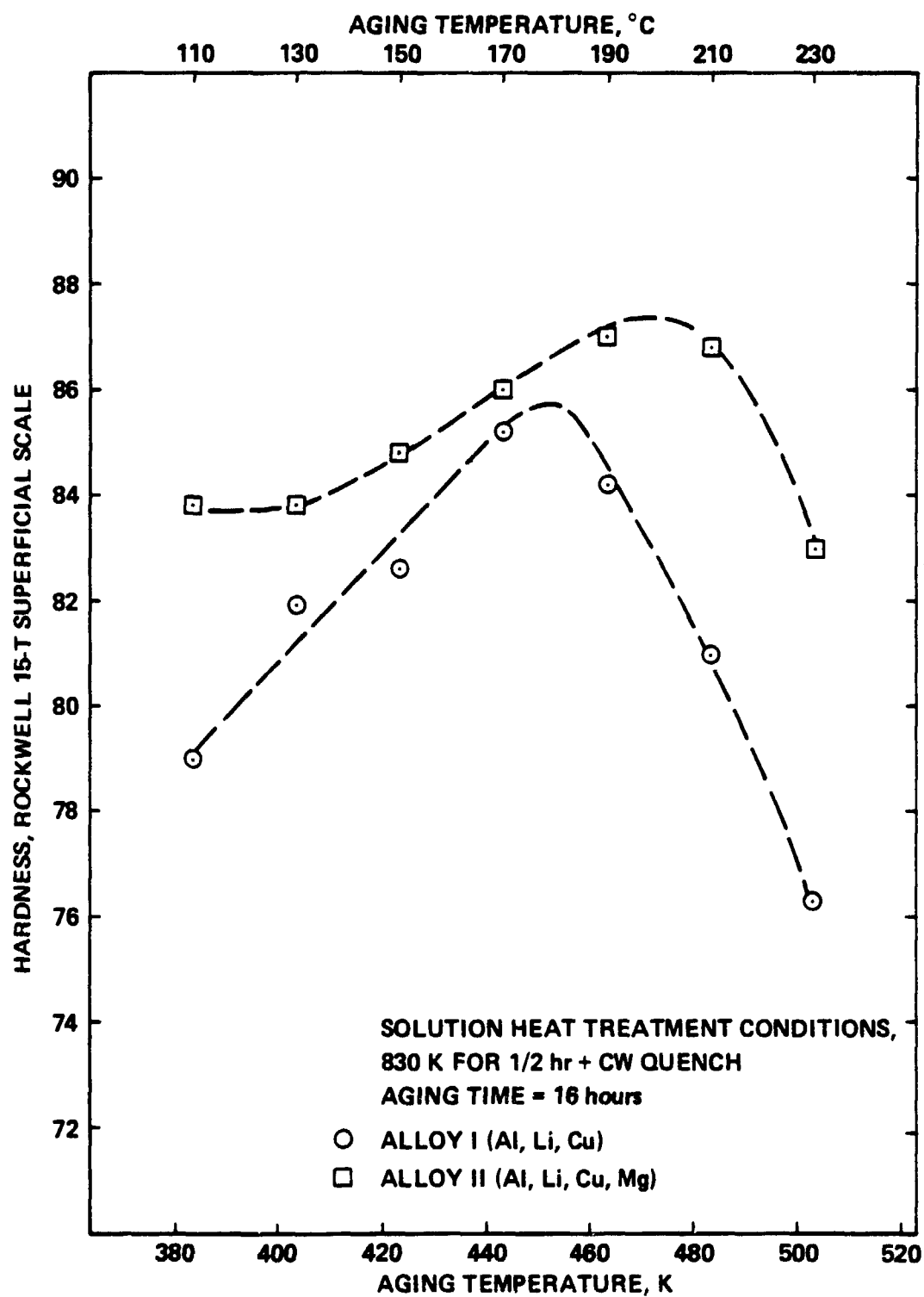
Fig. 7: Hardness as a function of aging temperature for a constant aging time of 16 hours.
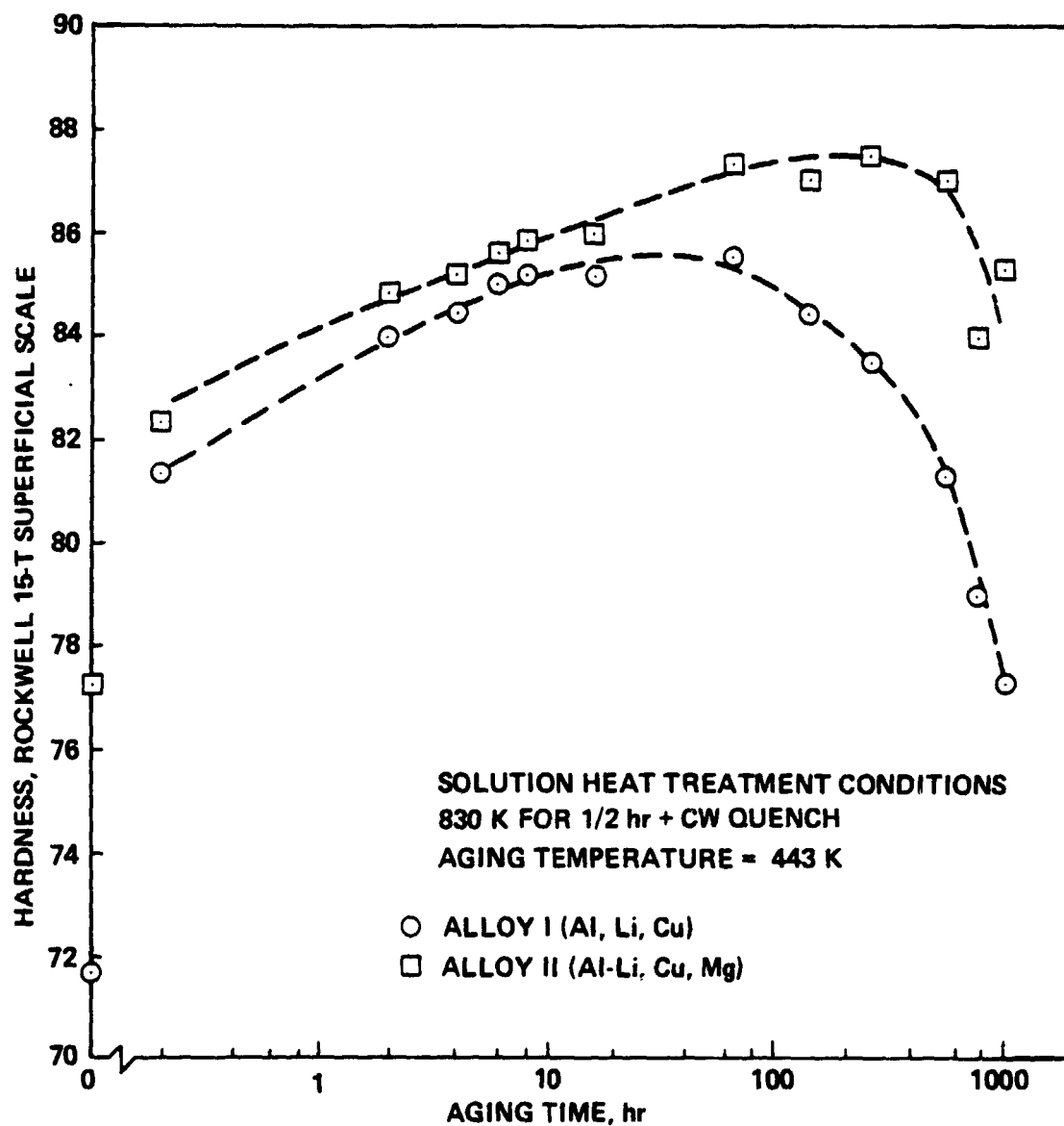
Fig. 8: Aging response of Alloys I and II at 443K (170C): hardness as a function of the time of aging.
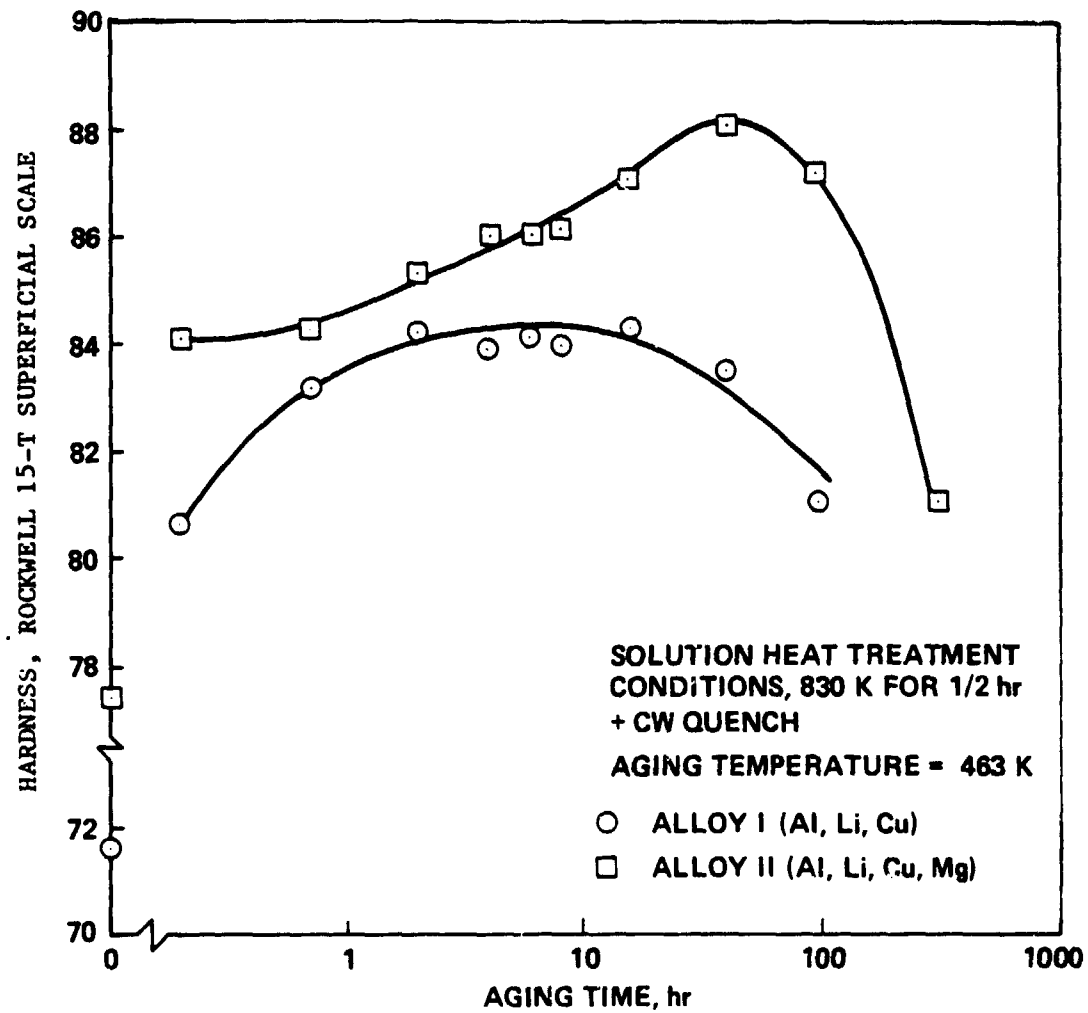
Fig. 9: Aging response of Alloys I and II at 463K (190C): hardness as a function of the time of aging.
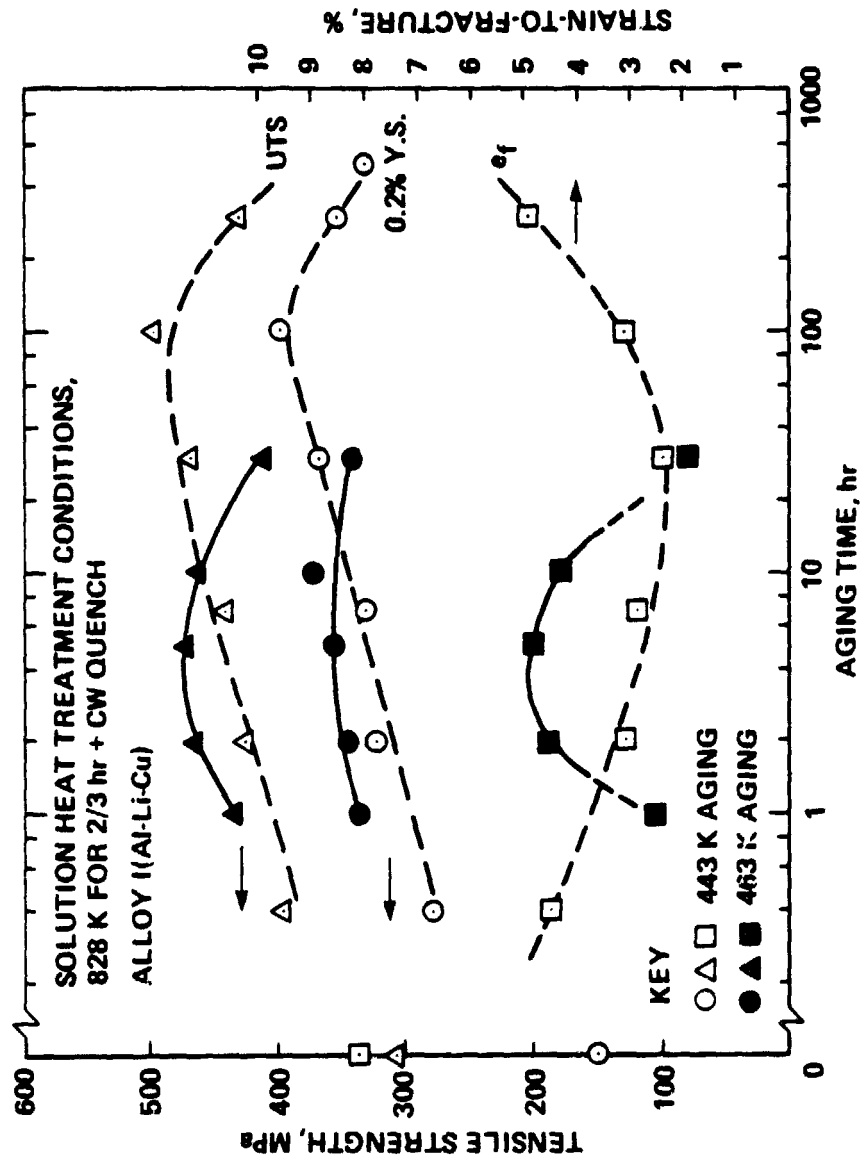
Fig. 10: Aging response of Alloy I hot-rolled sheet: tensile properties as a function of aging time at two aging temperatures – 443K and 463K.

37
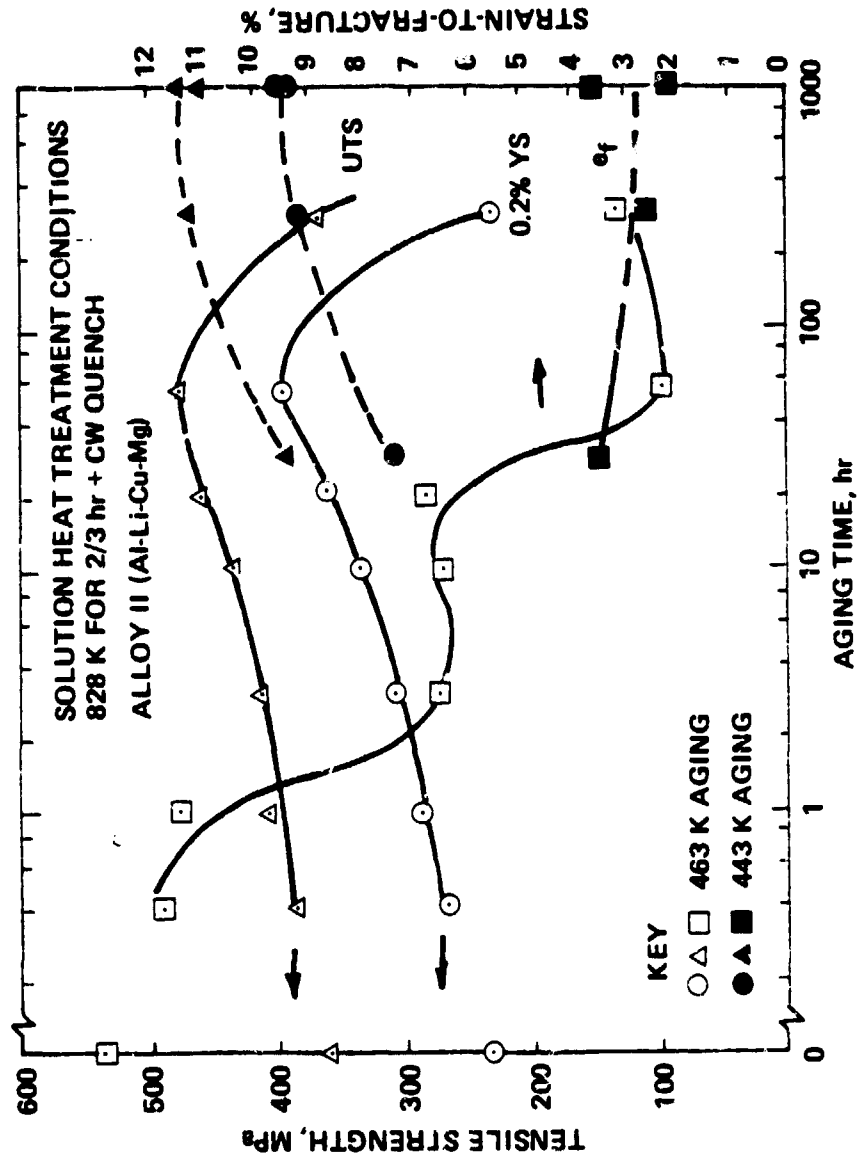
Fig. 11: Aging response of Alloy II hot-rolled sheet: tensile properties as a function of aging time at two aging temperatures – 443K and 463K.
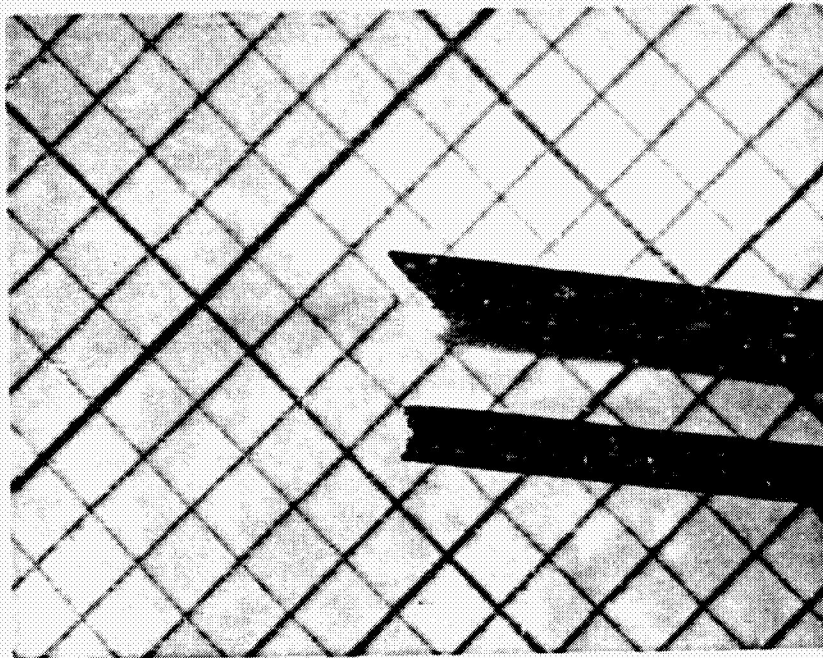
(a)   5X
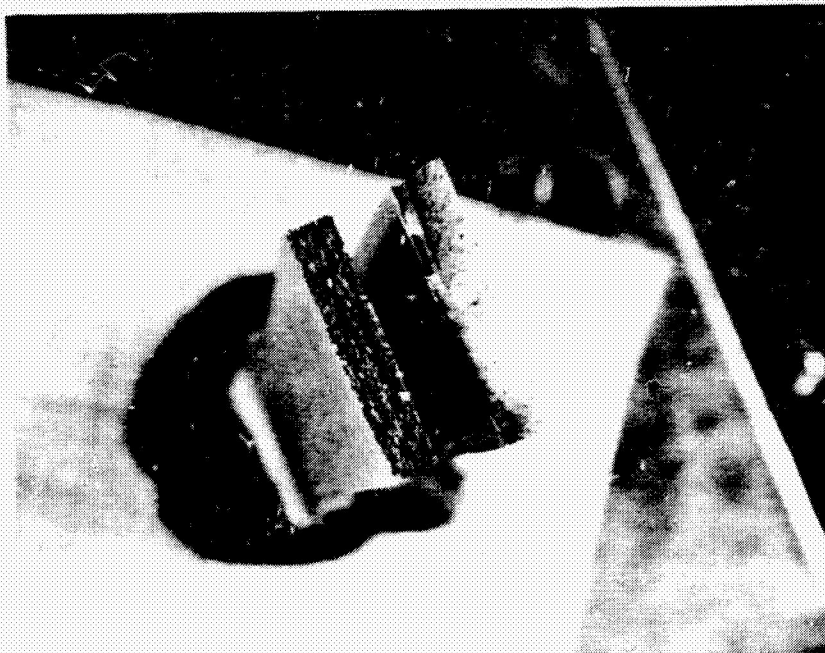
(b)   4.8X

Fig. 12:   The fracture morphology of tensile coupons fabricated
            from the hot-rolled strip (a) fracture profile, Alloy I
            (upper) versus Alloy II (lower) and (b) fracture surface
            comparison, Alloy I (right) versus Alloy II (left).

0.5mm

Fig. 13:   Scanning electron micrograph (SEM) of a fracture
           representative of that found for the hot-rolled
           Alloy I tensile coupons.

(a)

10μm

(b)
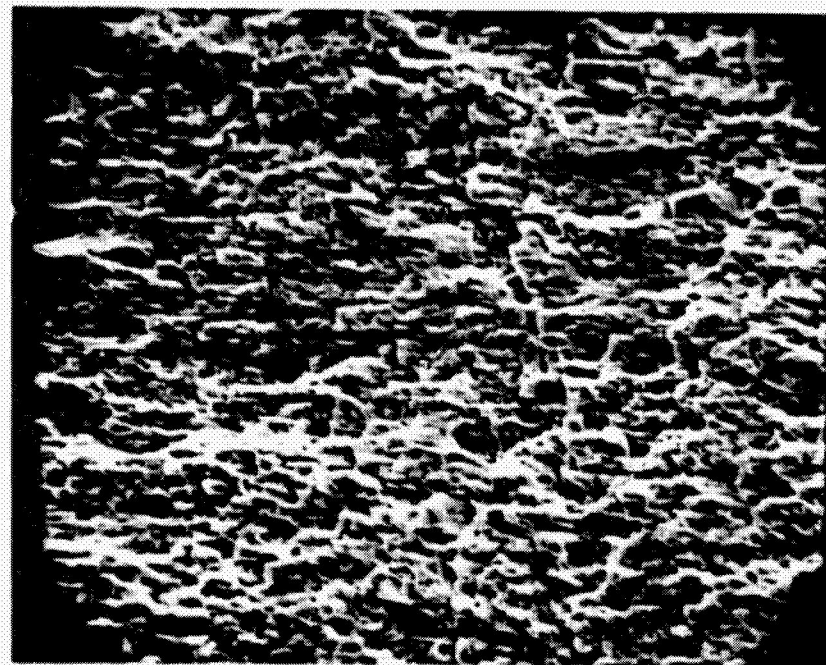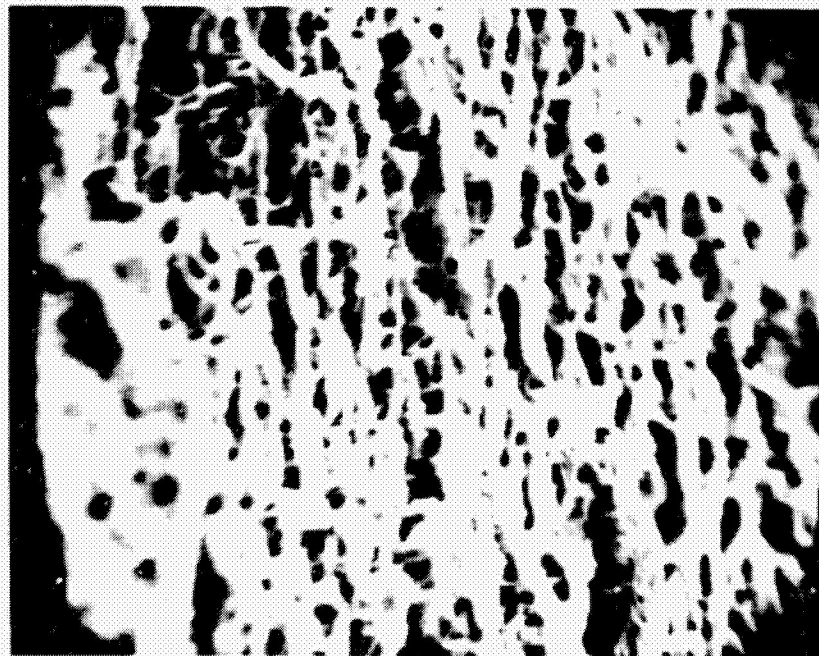
5μm

Fig. 14: Representative fractography (SEM) of the hot-rolled
Alloy I tensile fractures (a) characteristic fracture
topography (b) stepped features as viewed with side-
tilt.

0.5mm
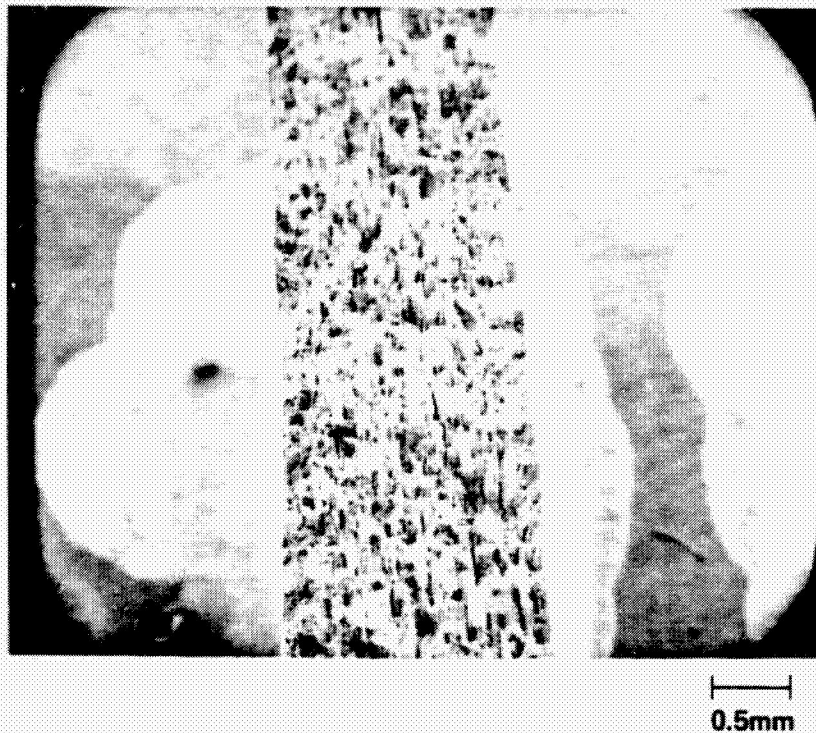
Fig. 15: Scanning electron micrograph (SEM) of a fracture
representative of that obtained in the hot-rolled
Alloy II (magnesium bearing) tensile coupons.

42

(a)

0.1mm
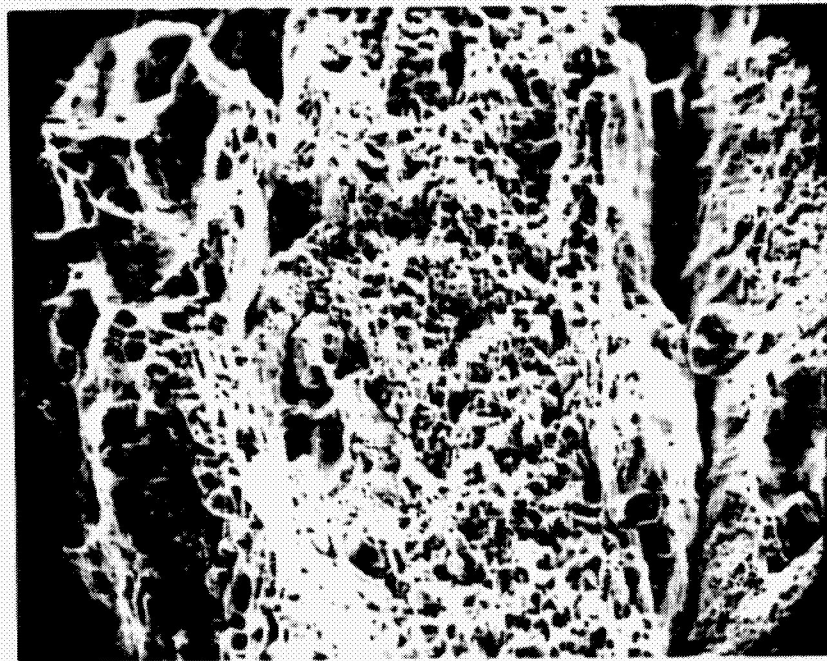
(b)

20μm

Fig. 16: Representative fractography (SEM) of the hot-rolled
Alloy II tensile fractures (a) high magnification of
the fracture depicted in Fig. 15 (b) further magnifi-
cation of the fracture (center region depicted in
micrograph (a).
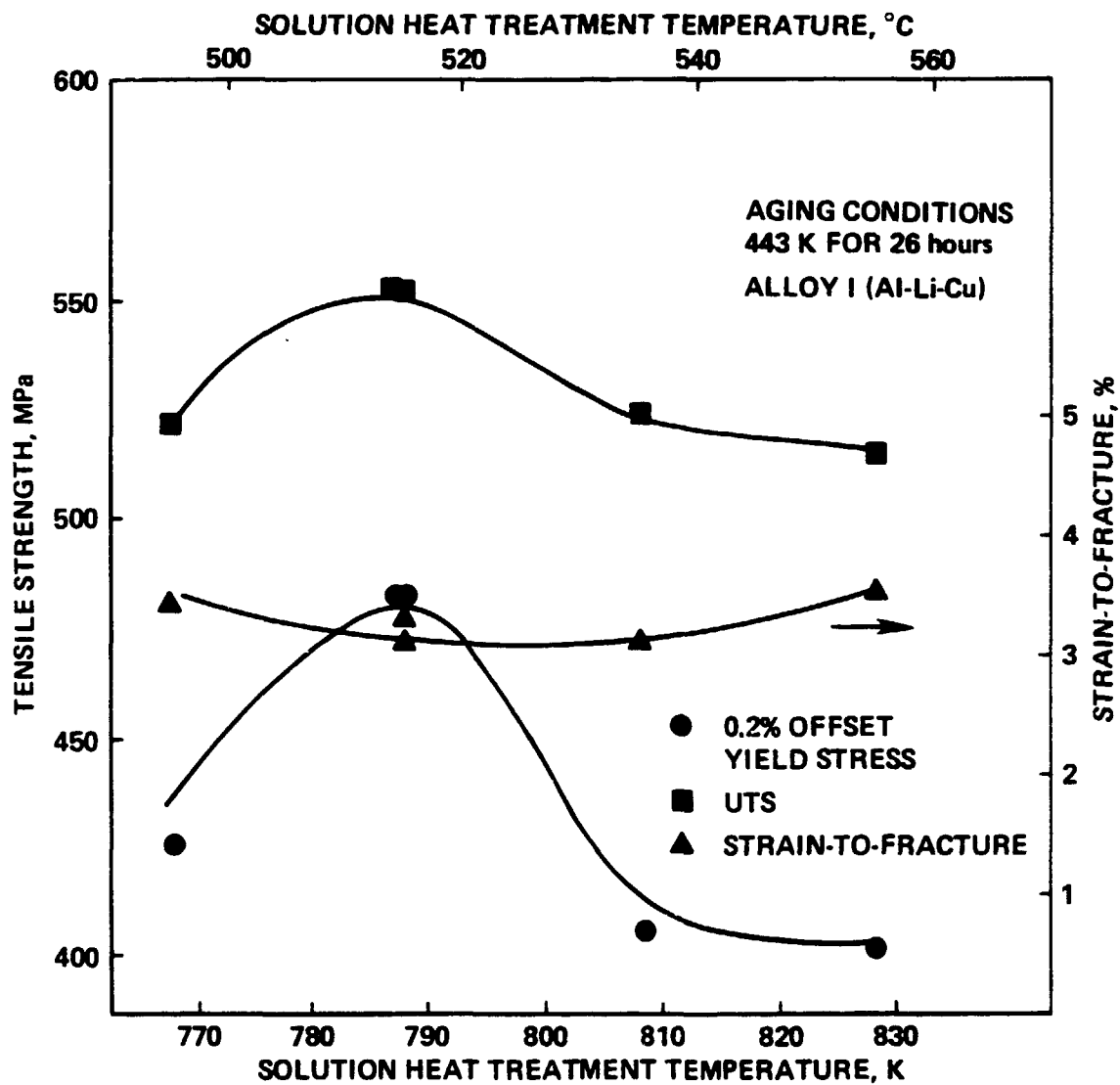
Fig. 17: The effect of solution heat treatment temperature on the tensile properties of as-extruded Alloy I for a constant aging condition.
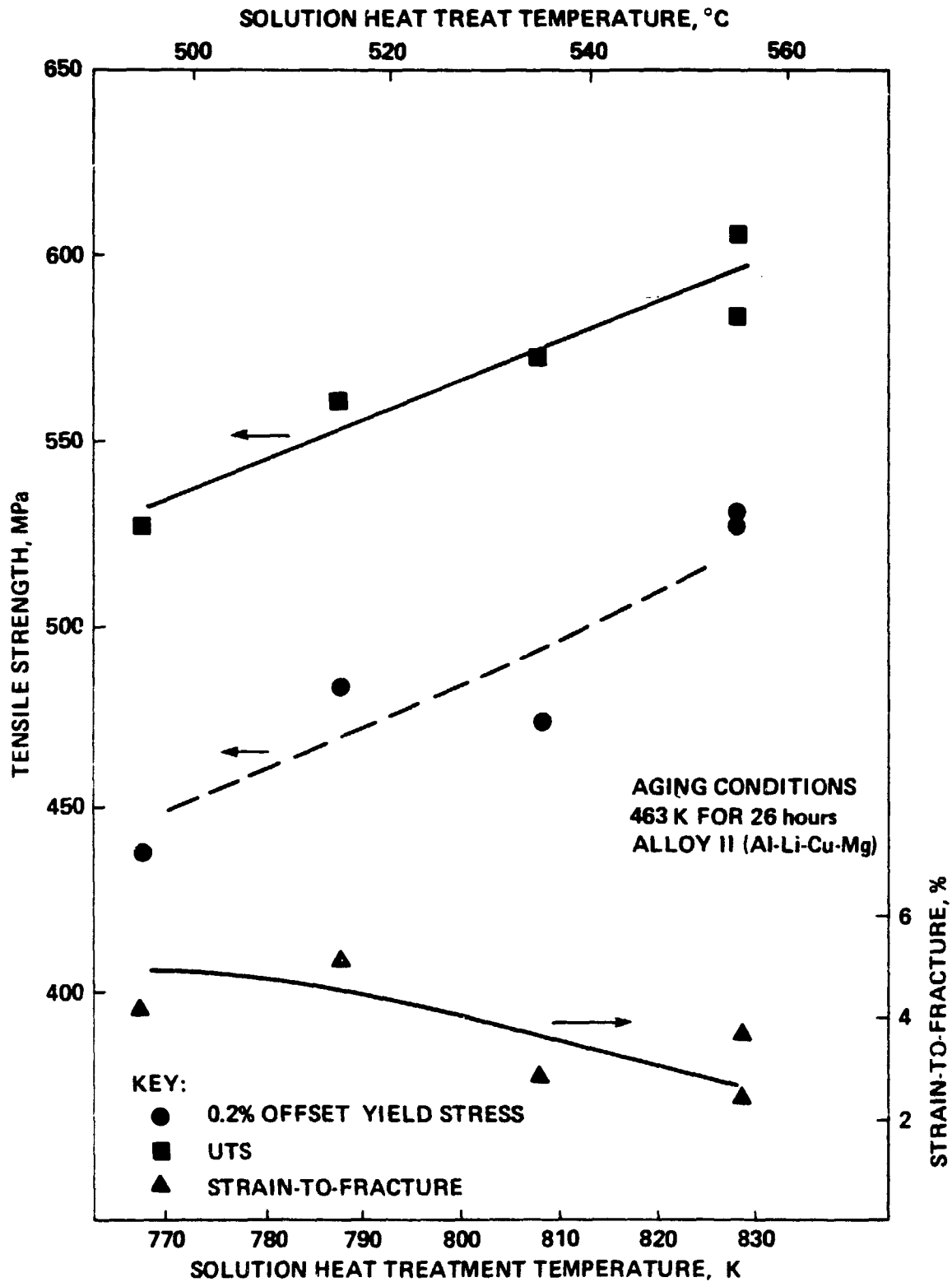
Fig. 18: The effect of solution heat treatment temperature on the tensile properties of as-extruded Alloy II for a constant aging condition.
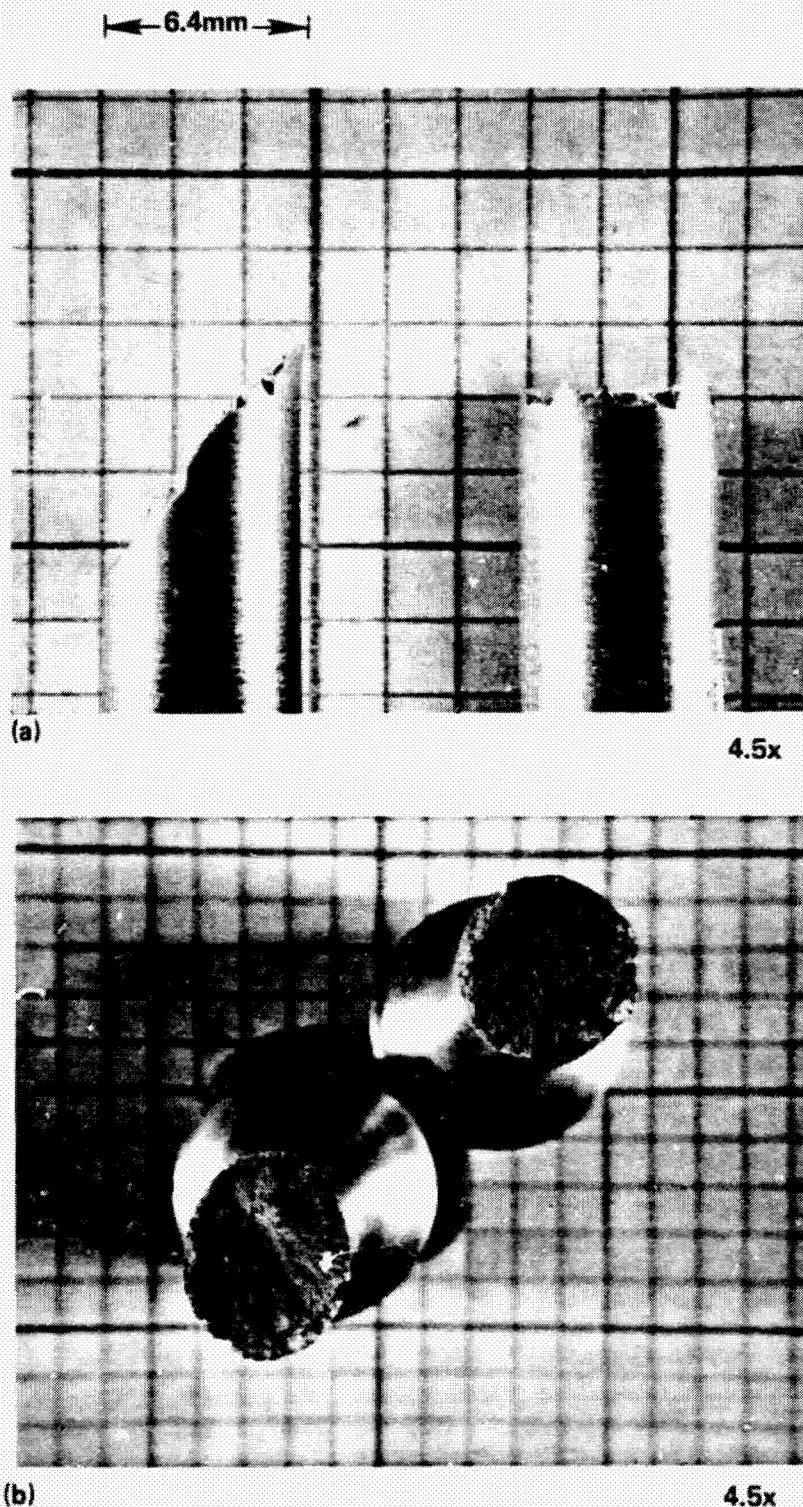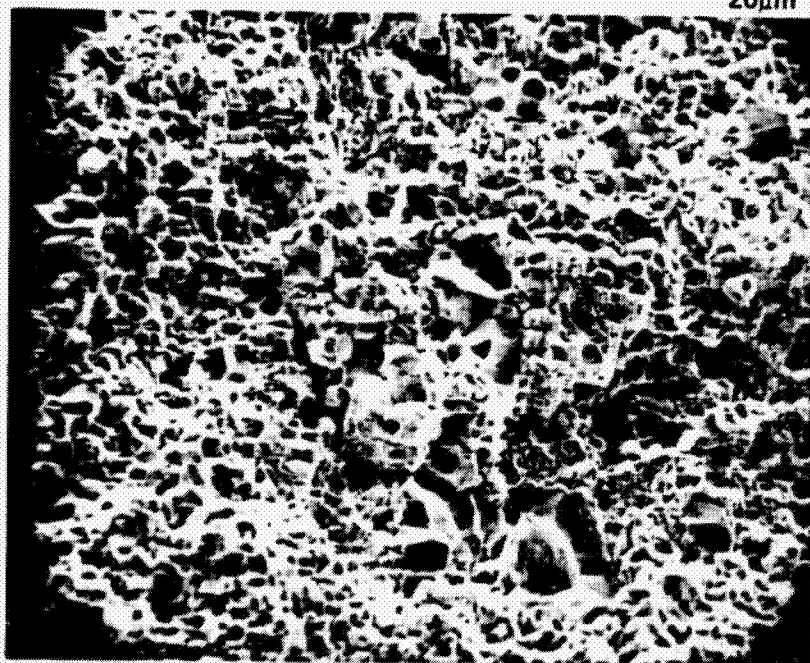
|← 6.4mm →|

(a)   4.5x

(b)   4.5x

Fig. 19:   The fracture morphology of tensile rounds fabricated
           from the as-extruded plate (a) fracture profile Alloy I
           (left) versus Alloy II (right) and (b) fracture surface
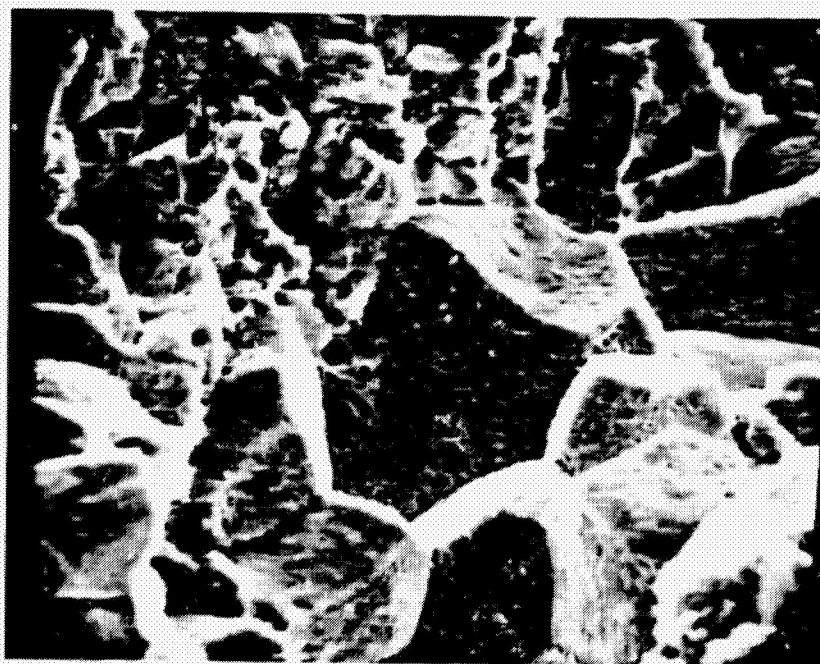   comparison, Alloy I (left) versus Alloy II (right).

46

Fig. 20: SEM comparison of the shear fracture topography, Alloy I, to the tensile fracture topography of Alloy II for tensile round specimens fabricated from the as-extruded plate (a) stepped shear topography characteristic of Alloy I (b) intergranular fracture observed in Alloy II.
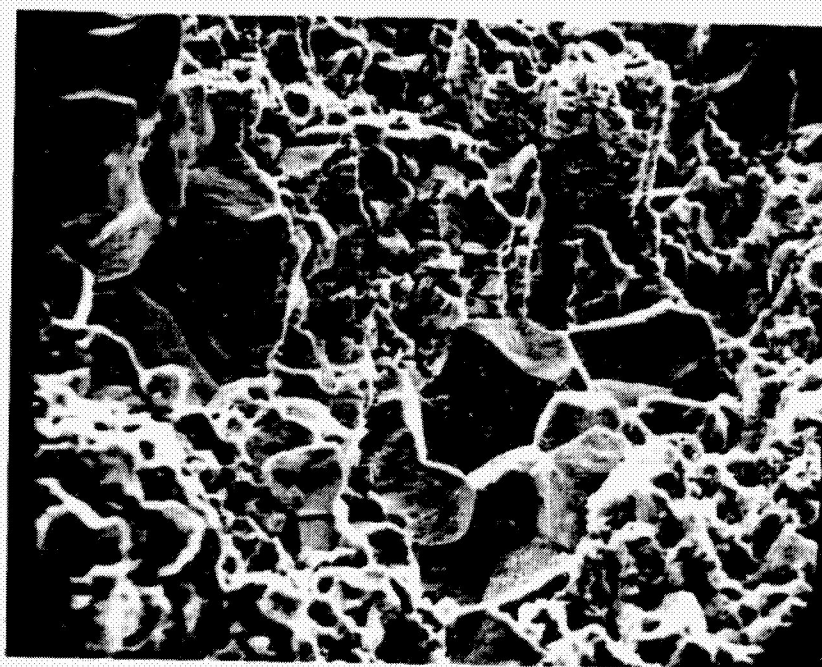
(a)

10μm

(b)

5μm

Fig. 21:   Intergranular fracture of Alloy II (Al-Li-Cu-Mg)
           (a) intergranular facets and secondary cracks (b)
           two-fold magnification of the faceted region in (a),
           above, depicting extensive grain boundary precipi-
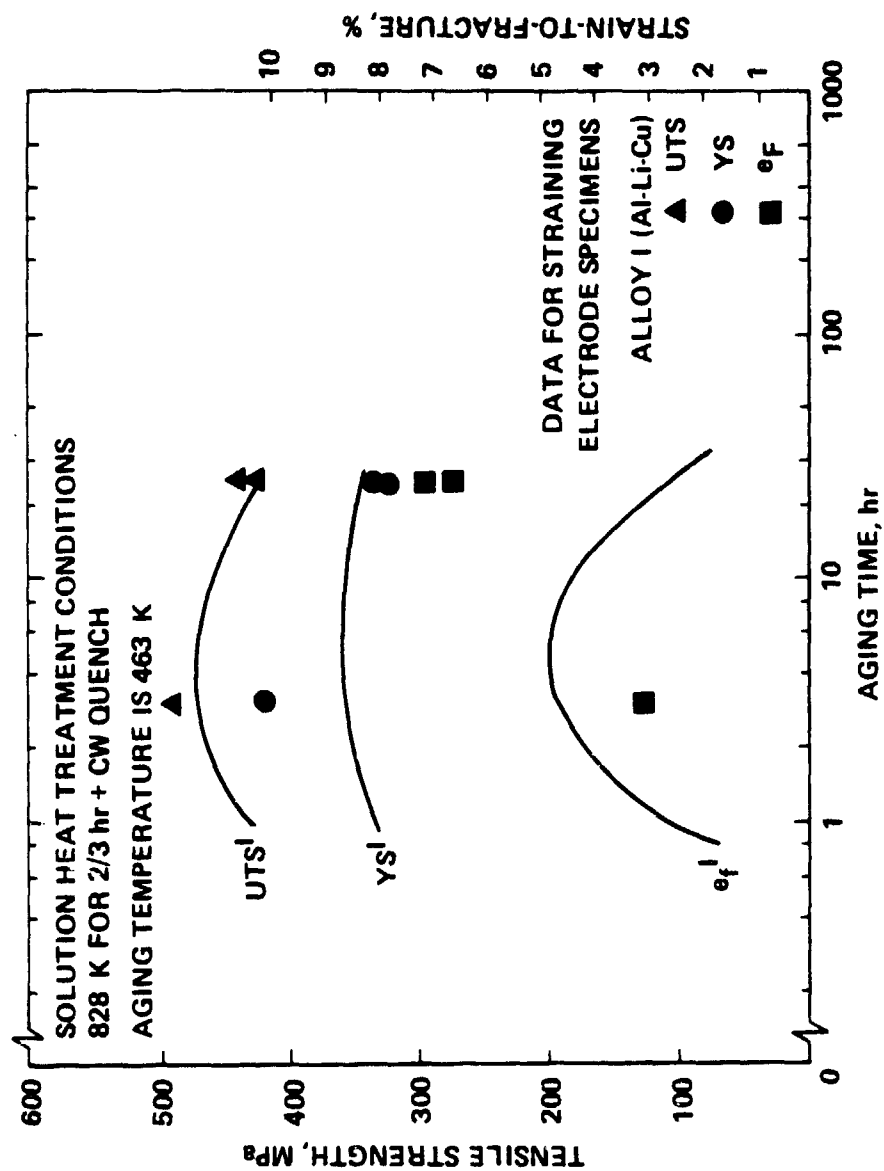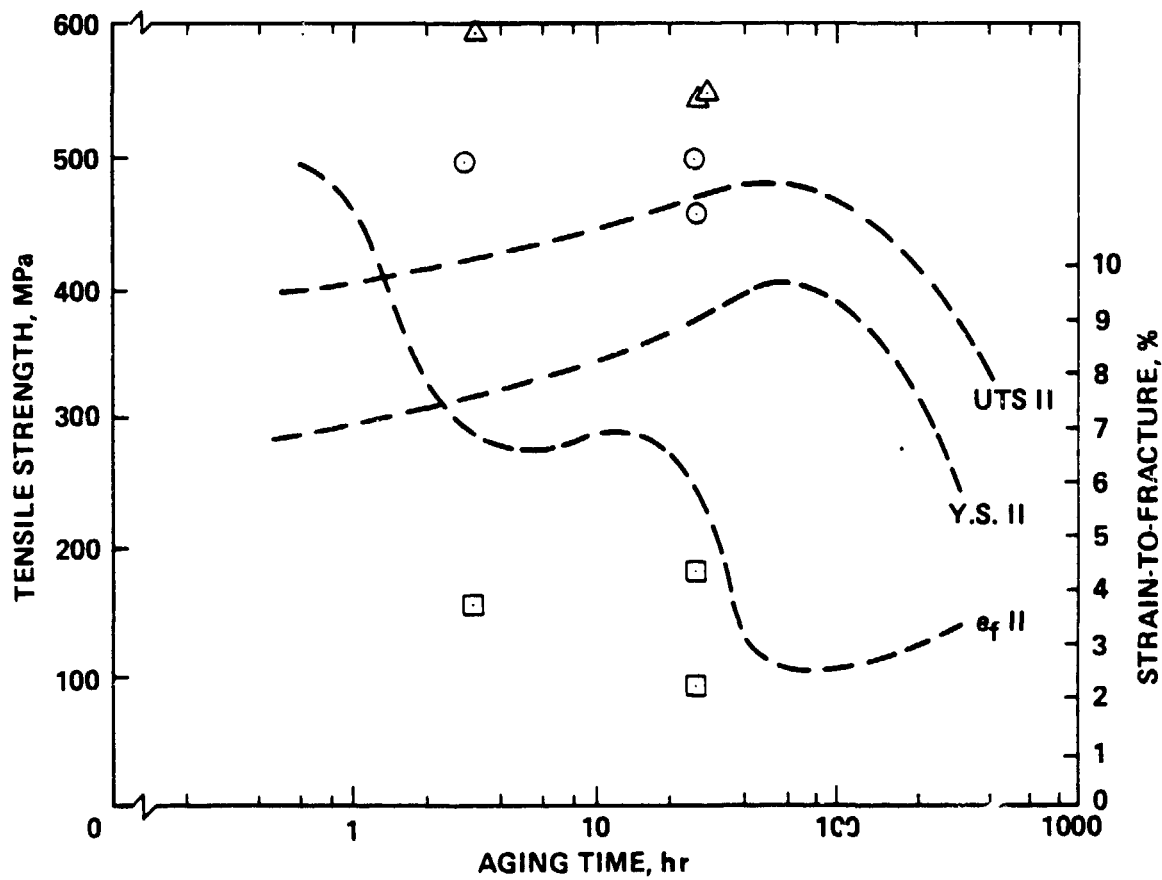   tation.

48

Fig. 22: A comparison of Alloy I straining electrode specimen data to the aging response curves obtained from tensile coupons, Fig. 10.

SOLUTION HEAT TREATMENT CONDITIONS
828 K FOR 2/3 hr + CW QUENCH

FINAL AGING TEMPERATURE IS 463 K

DATA FOR STRAINING ELECTRODE SPECIMENS

KEY   ALLOY II, DUPLEX AGED

△ UTS
○ Y.S.
□ e_f

Fig. 23:   A comparison cf Alloy II straining electrode specimen
data to the aging response curves obtained from
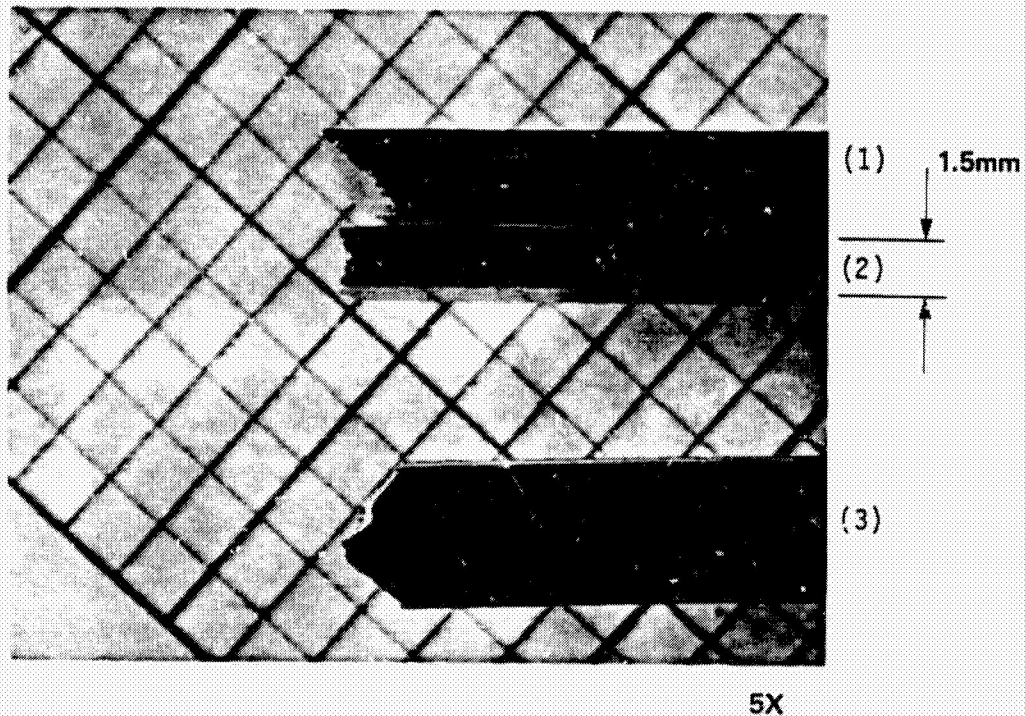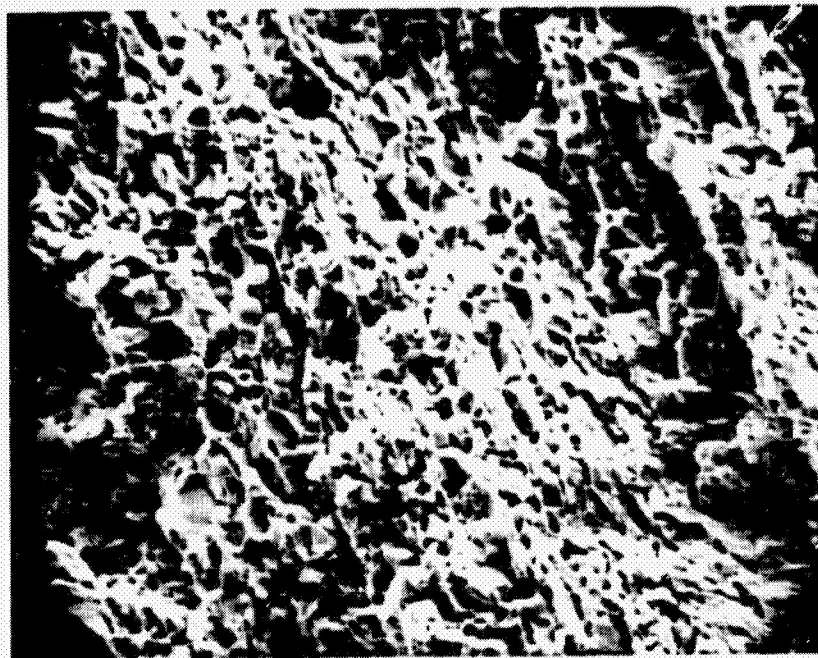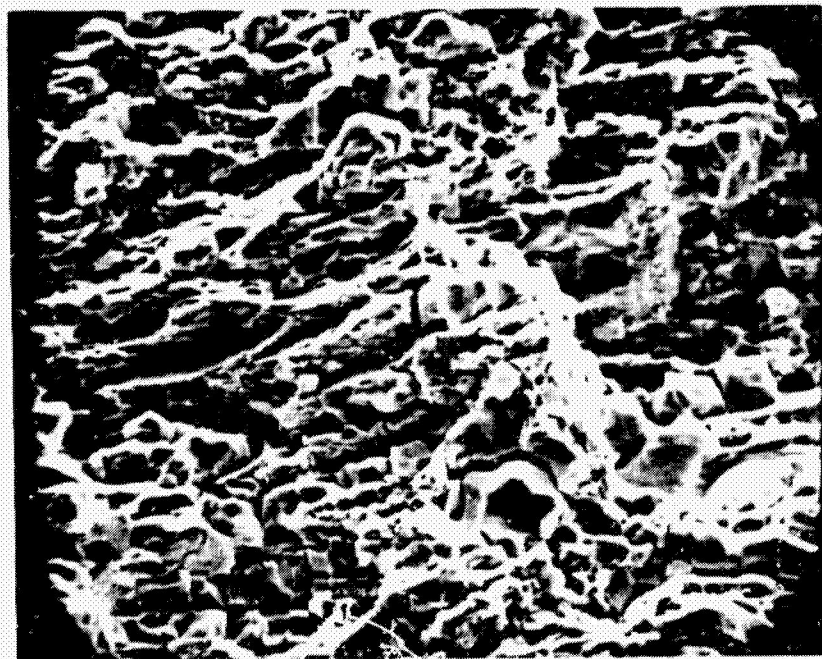tensile coupons, Fig. 11.

50

5X

Fig. 24: A comparison of fracture profiles of three specimens
(1) shear fracture of an Alloy I tensile coupon (top)
(2) tensile fracture and an Alloy II tensile coupon
(center), and (3) double shear fracture of a straining
electrode type specimen, Alloy I (bottom).

51

(a)

10μm

(b)

10μm

Fig. 25:   SEM comparison of the shear fracture topography,
          Alloy I, to the tensile fracture topography of Alloy II
          for straining electrode specimens fabricated from the
          as-extruded plate (a) stepped shear topography, Alloy I
          (b) grain boundary faceting and secondary cracking,
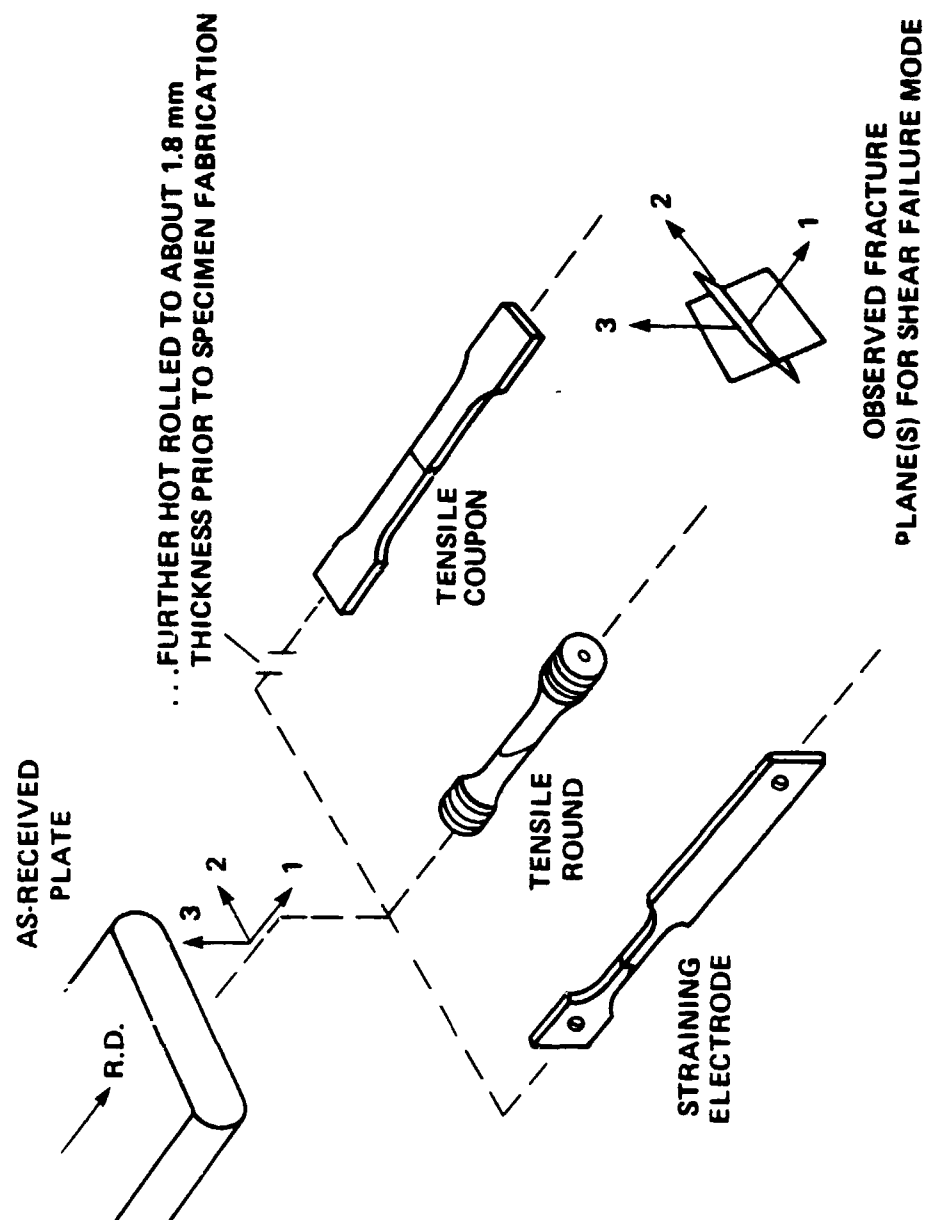   characteristic of Alloy II.

52

Fig. 26: The orientational relationship between the shear fracture plane(s) and the extrusion direction (E.D.) of the as-received Al-Li alloy plate.

53

Table I Chemical Composition of the Aluminum-Lithium
Alloys Selected for this Study

Program Designation	KBI Alloy Designation	Wt. Pct.											ppm		
		Li	Cu	Mg	Zr	Si	Fe	Mn	Zn	Ti	Cr	Be	Ca	Na	K
Alloy I	80001	2.6	1.4	.006	.09	.03	.06	<.005	<.02	<.03	<.002	<.005	<3	2	1
Alloy II	80002	2.6	1.4	1.6	.09	.03	.05	<.005	<.02	<.03	<.002	<.005	<3	1	1

Table II   Young's Modulus Comparison Data

$E_{Alloy\ I}$ = 80.0 GPa

$E_{Alloy\ II}$ = 80.7 GPa

$E_{7075-T6\ Aluminium}$ = 71.7 GPa

Note: a) Alloys I and II in peak-aged condition.

b) Modulus determinations made from the output
of two strain gages on opposite sides of flat
tensile coupons.

c) 7075-T6 Modulus value reported in Aluminum
Standards and Data - 1979, The Aluminum
Association (Sixth Edition), March 1979.